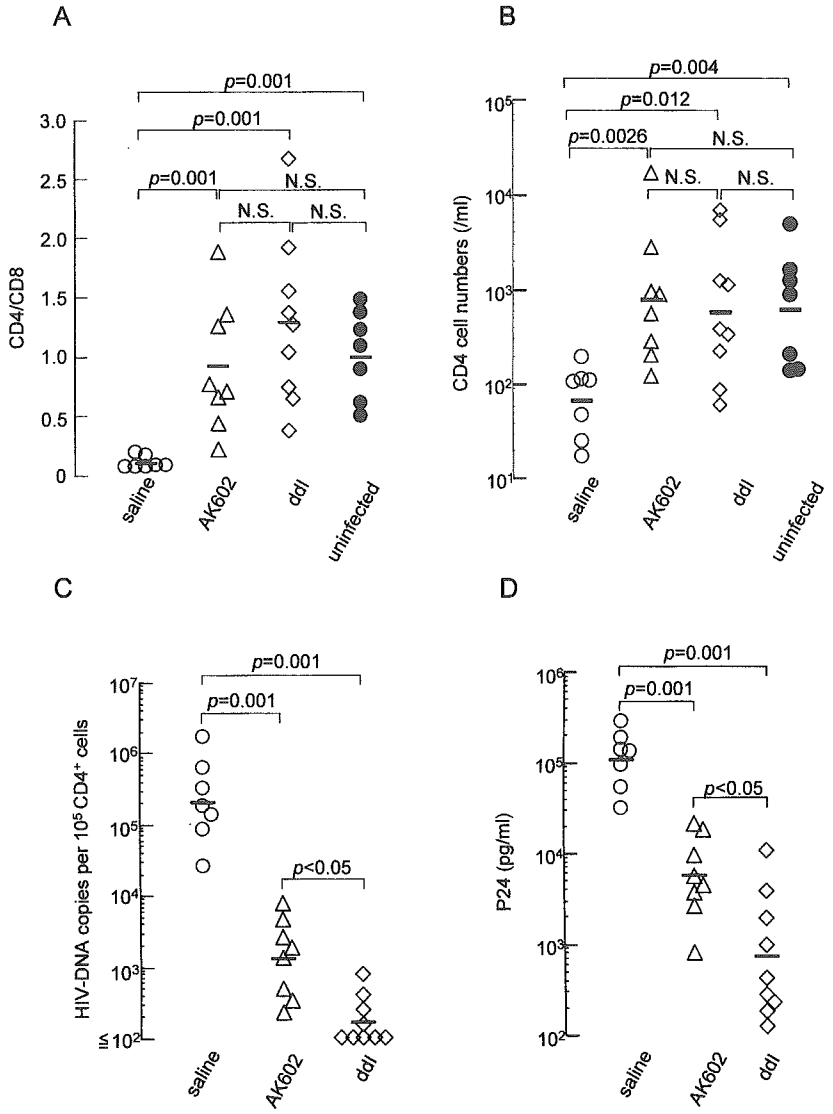

FIG. 6. Effects of AK602 on $CD4^+/CD8^+$ ratios and the amounts of proviral DNA and HIV-1 p24 in infected hu-PBMC-NOG mice. (A) Overall profiles of $CD4^+/CD8^+$ cell ratios. Note that the mean $CD4^+/CD8^+$ cell ratio in mice given saline ($n = 7$) was 0.1, while those in mice given AK602 or ddI were 0.92 and 1.29, respectively. The mean ratio in uninfected mice was 1.0. (B) Numbers of $CD4^+$ cells per microliter in each mouse group. (C) HIV-1 proviral DNA copy numbers in $CD4^+$ cells from each mouse group were determined by real-time PCR assay. Values are shown per 10^5 $CD4^+$ cells, as described in Materials and Methods. Note that the mean number of HIV-1 proviral DNA copies was 2.0×10^5 per 10^5 $CD4^+$ cells in mice given saline, while those in AK602- and ddI-treated groups were 1.3×10^3 and 1.8×10^2 per 10^5 $CD4^+$ cells (both, $P = 0.001$), respectively. (D) Amounts of plasma p24 antigen. Note that the amounts of p24 in plasma were high in saline-treated mice while AK602 and ddI significantly suppressed the serum p24 amounts as examined on day 16 after $HIV\text{-}1_{Ba\text{-}L}$ inoculation. The short bars indicate the arithmetic (A) and geometric (B, C, and D) means obtained.

levels of HLA-DR, and rapidly and continuously proliferated immediately after intraperitoneal infusion (Fig. 3A, B, and D). Moreover, the implanted PBMC expressed as much as 2.8-fold-higher levels of CCR5 on day 3 following implantation compared to PHA-PBMC on day 3 in culture (Fig. 3E). The combination of rapid proliferation and high levels of CCR5 expression of the implanted PBMC should explain the reason R5 HIV-1 rapidly replicated in the hu-PBMC-NOG mice and presented such high levels of R5 HIV-1 viremia. In this regard, only a few groups to date have documented the levels of viremia in the scientific literature. Among them are those by Garaci et al. (8) and Koyanagi et al. (14). The former documented high levels of viremia with a peak of 2.67×10^6 copies/ml in hu-PBL-NOD-SCID mice in which HIV-1-infected macrophages were inoculated, unlike our NOG mouse model where HIV-1 was directly inoculated. The latter report by Koyanagi et al. does not have viremia data but has data on p24 levels with a geometric mean of 11,092 pg/ml on day 14 after HIV-1 inoculation. However, the variation was much greater (178 to 1,434,444 pg/ml). Thus, one can say that the present model provides a greater reproducibility of high viremia levels than the mouse system reported by Koyanagi (14). It should be noted that the high levels of viremia and high engraftment rate achieved in this mouse model made it possible to monitor the

TABLE 2. Comparison of HIV-1 proviral DNA in human $CD4^+$ and $CD4^-$ cell fractions[a]

Sample	HIV-1 DNA copies (10^5 cells)		
	SCID-PBMC	$CD4^+$ cells	$CD4^-$ cells
Saline 1	138,858	162,193	461
Saline 2	135,967	117,949	<100
Saline 3	83,863	94,590	<100
AK602 1	3,390	2,300	<100
AK602 2	5,575	4,606	<100
AK602 3	1,925	1,398	<100
ddI 1	301	516	<100
ddI 2	793	1,317	<100
ddI 3	<100	118	<100

[a] HIV-1 proviral DNA copy numbers were determined by real-time PCR assay of unseparated human PBMC and purified $CD4^+$ and $CD4^-$ cells, following recovery from hu-PBMC-NOG mice. Values are shown per 10^5 cells, as described in Materials and Methods.

changes in the viremia levels periodically in the same set of mice without sacrificing them, while most of the previously described SCID mouse models required mice to be sacrificed at each time point of testing (25, 29, 30) or needed further in vitro coculture of the PBMC recovered from the mice with freshly prepared uninfected target cells for an additional period of days (9, 34).

We demonstrated in this study that a novel SDP derivative, AK602, exerted highly potent activity against laboratory and primary R5 HIV-1 strains as well as MDR R5 HIV-1 variant with IC_{50} values of subnanomolar concentrations (Table 1). It should be noted that AK602 represents a novel SDP derivative, which binds to human CCR5 but not to human CXCR4, CCR1, CCR2, CCR3, CCR4 or murine CCR5; blocks the binding of MIP-1α to CCR5 with an extremely high affinity (K_d values of ~3 nM); potently blocks HIV-1-gp120/CCR5 binding; and exerts potent activity against a wide spectrum of laboratory and primary R5 HIV-1 isolates including MDR HIV-1 and HIV-1 strains of various clades with IC_{50} values of 0.2 to 0.6 nM in vitro (K. Maeda, H. Ogata, S. Harada, Y. Tojo, T. Miyakawa, H. Nakata, Y. Takaoka, S. Shibayama, D. Fukushima, J. Moravek, E. Arnold, and H. Mitsuya, 11th Conf. Retrovir. Opp. Infect., abstr. 540, 2004; J. Demarest et al., XV Int. AIDS Conf., abstr. WeOrA1231, 2004). The plasma half-life of AK602 in the hu-PBMC-NOG mice, however, proved to be as short as 29 min when the agent was administered intraperitoneally (Fig. 4A). Considering that AK602 possesses such a high binding affinity to CCR5, we presumed that AK602 could remain on CCR5 for an extended period of time even after the agent was removed from the bloodstream in mice. The high and extensive level of AK602 occupancy observed in PBMC recovered from mice receiving AK602 substantiated this presumption (Fig. 4D). The subsequent in vitro experiment in which $CCR5^+$ MAGI cells were incubated with AK602 but exposed to R5 HIV-1 after the removal of the compound from the culture medium showed that AK602's anti-R5 HIV-1 activity can persist for an extensive period of time even if AK602 is no longer present in the culture (Fig. 4E). It is of note that unlike certain reports of in vivo anti-HIV-1 activity of chemokine antagonists which were administered before HIV-1 inoculation, thus demonstrating prophylactic effects of such agents (9, 30), the present system demonstrates anti-HIV-1 treatment after the establishment of HIV-1 infection, analogous to antiviral therapy in clinical settings.

When highly active antiretroviral therapy exerts its potent antiviral effects in clinical settings, a decrease in HIV-1 viremia is seen often within weeks, ultimately resulting in undetectable viremia; however in the present study, the viremia levels in mice receiving AK602 or ddI continued to increase although the rate of increment significantly declined (Fig. 7). The failure of AK602 and ddI to decrease viremia levels could be due in part to such a rapid viral replication in hyperactivated and proliferating $CD4^+$ cells. As discussed earlier, PBMC recovered from the hu-PBMC-NOG mice were highly positive for CCR5 and HLA-DR (Fig. 3D and E), compared to the levels of activation seen in the same donor's PHA-PBMC. It should be noted, however, that the mean numbers of proviral DNA copies on day 16 in mice receiving AK602 and ddI were 1.3×10^3 and 1.8×10^2 per 10^5 $CD4^+$ cells, respectively (Fig. 6C), suggesting that most $CD4^+$ cells (98.7 and 99.8% on average, respectively) were free of HIV-1 and proliferating in those

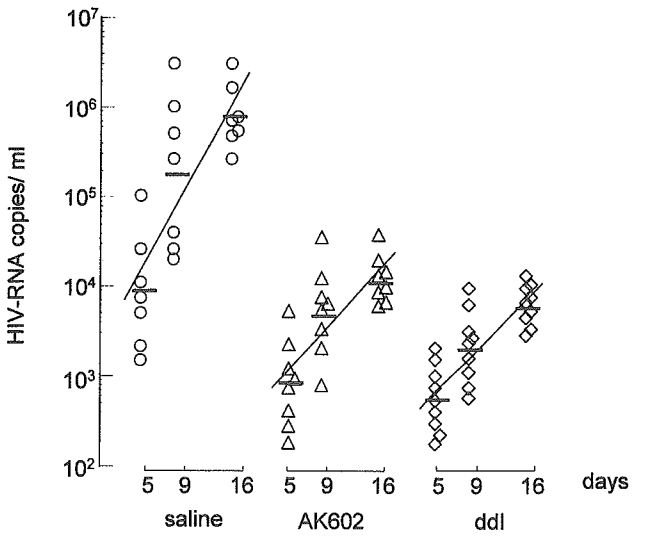

FIG. 7. AK602 suppresses R5 HIV-1 viremia in hu-PBMC-NOG mice. Blood samples were collected on days 5, 9, and 16 after inoculation and were subjected to the determination of R5 HIV-1 RNA copy numbers. Note that the copy numbers in saline-treated mice rapidly increased and reached ~10^6/ml by day 16, while AK602 significantly suppressed the viremia by 1.6 and 1.8 logs as examined on day 9 ($P = 0.001$ compared to saline-treated mice) and day 16 ($P = 0.001$), respectively. Comparable viremia suppression was seen in ddI-treated mice, except on day 16, when ddI activity was greater than that of AK602 ($P = 0.027$). Note that there was a clear reduction in the rate of increase of viremia as well. When the values of $\log_{10}$ HIV-1 RNA copies were calculated and the slopes corresponding to the rates of increase per day were determined, the resulting mean slope (solid line) for the saline-treated mice was 0.167 ± 0.042, whereas those for the AK602- and ddI-treated mice were 0.102 ± 0.041 and 0.091 ± 0.037, respectively. The increase rate for saline-treated mice was significantly higher than those of AK602-treated mice ($P = 0.0057$) and ddI-treated mice ($P = 0.0023$), respectively. The horizontal bars and solid lines represent the geometric means of HIV-1 RNA copy numbers and the slopes calculated, respectively.

mice on day 16 after the virus inoculation, if one copy of proviral DNA was postulated to reside in one $CD4^+$ cell.

One of us (Y.K.) previously attempted to investigate the mechanism of $CD4^+$ cell depletion seen in individuals with HIV-1 infection by employing a PBMC-transplanted NOD (NOD/Shi) *scid/scid* mouse system (24). Massive apoptosis was observed in HIV-1-uninfected $CD4^+$ cells in the spleens of the HIV-1-infected NOD-*scid/scid* mice. A combination of terminal deoxynucleotidyl transferase-mediated dUTP nick-end labeling and immunostaining for death-inducing tumor necrosis factor (TNF) family molecules showed that apoptotic cells were frequently found in conjugation with TNF-related apoptosis-inducing ligand (TRAIL)-expressing $CD3^+$ $CD4^+$ human T cells. Further observation that a neutralizing anti-TRAIL antibody inhibited the development of $CD4^+$ cell apoptosis suggested that a large number of HIV-1-uninfected $CD4^+$ cells undergo TRAIL-mediated apoptosis, contributing to the marked depletion of $CD4^+$ cells (24). The observation by Miura and his colleagues that the number of TRAIL-positive cells was consistently higher in HIV-1-infected mice than in uninfected ones makes it apparent that TRAIL expression is induced upon HIV-1 infection (23, 24). In this regard, the present observation that AK602 and ddI potently blocked the decrease in $CD4^+$ cells in spite of the rather increasing HIV-1 viremia in the face of AK602 or ddI (Fig. 7) suggests that the mere presence of viremia might not be sufficient for the HIV-induced apoptosis in $CD4^+$ cells. Our observation that most surviving $CD4^+$ cells in mice receiving AK602 or ddI were free of HIV-1 (see above) suggests that these anti-HIV-1 agents might block not only de novo HIV-1 infection, but also bystander killing of uninfected $CD4^+$ cells. The present data also suggest that a certain factor(s) such as cytokines produced by the freshly HIV-1-infected cells might mediate the apoptosis of bystander $CD4^+$ cells through the upregulation of TRAIL expression, death receptors (e.g., DR4 and DR5), and/or downregulation of decoy receptors (e.g., DcR1 and DcR2) (26, 27). However, experiments with a combination of terminal deoxynucleotidyl transferase-mediated dUTP nick-end labeling and TNF family molecules have to be conducted for better understanding of the bystander killing in regard to AK602's effects.

It is of note that several CCR5 antagonists are currently in various stages of development. AK602 has recently been administered to healthy adult subjects in a phase I clinical trial and shown to bind to CCR5 for an extended period of time, suggesting that an oral formulation with fewer administrations and lower dosage is possible for AK602 as a therapeutic agent for HIV-1 infection (J. Demarest, K. Adkison, S. Sparks, A. Shachoy-Clark, K. Schell, S. Reddy, L. Fang, K. O'Mara, S. Shibayama, and S. Piscitelli, 11th Conf. Retrovir. Opp. Infect., abstr. 139, 2004). Taken together, our observations that plasma viral load reached $\sim 10^6$ RNA copies/ml and that AK602 potently inhibited the replication of R5 HIV-1 strongly suggest that the present hu-PBMC-NOG mouse AIDS model could serve as a useful instrument for analyzing the pathogenesis of HIV-1 infection and testing the efficacy of antiviral agents.

ACKNOWLEDGMENTS

We thank Seth Steinberg for statistical analysis and Naoko Misawa, Yuji Kawano, and Hiromi Ogata for technical assistance and discussion.

This work was supported in part by grant-in-aids for Scientific Research on Priority Areas (14207025 and 15019086) from the Japanese Ministry of Education, Science, Sports, Culture and Technology of Japan (Monbu-Kagakusho) and a grant for AIDS Research (H15-AIDS-001) from the Ministry of Health, Labor, and Welfare of Japan (Kosei-Rohdosho).

REFERENCES

1. **Baba, M., O. Nishimura, N. Kanzaki, M. Okamoto, H. Sawada, Y. Iizawa, M. Shiraishi, Y. Aramaki, K. Okonogi, Y. Ogawa, K. Meguro, and M. Fujino.** 1999. A small-molecule, nonpeptide CCR5 antagonist with highly potent and selective anti HIV-1 activity. Proc. Natl. Acad. Sci. USA **96:**5698–5703.
2. **Carr, A., K. Samaras, A. Thorisdottir, G. R. Kaufmann, D. J. Chisholm, and D. A. Cooper.** 1999. Diagnosis, prediction, and natural course of HIV-1 protease-inhibitor associated lipodystrophy, hyperlipidaemia, and diabetes mellitus: a cohort study. Lancet **353:**2093–2099.
3. **Dean, M., M. Carrington, C. Winkler, G. A. Huttley, M. W. Smith, R. Allikmets, J. J. Goedert, S. P. Buchbinder, E. Vittinghoff, E. Gomperts, S. Donfield, D. Vlahov, R. Kaslow, A. Saah, C. Rinaldo, R. Detels, and S. J. O'Brien.** 1996. Genetic restriction of HIV-1 infection and progression to AIDS by a deletion allele of the CKR5 structural gene. Hemophilia Growth and Development Study, Multicenter AIDS Cohort Study, Multicenter Hemophilia Cohort Study, San Francisco City Cohort, ALIVE Study. Science **273:**1856–1862.
4. **Easterbrook, P. J.** 1999. Long-term non-progression in HIV infection: definitions and epidemiological issues. J. Infect. **38:**71–73.
5. **Fauci, A. S.** 1999. The AIDS epidemic—considerations for the 21st century. N. Engl. J. Med. **341:**1046–1050.
6. **Finzi, D., J. Blankson, J. D. Siliciano, J. B. Margolick, K. Chadwick, T. Pierson, K. Smith, J. Lisziewicz, F. Lori, C. Flexner, T. C. Quinn, R. E. Chaisson, E. Rosenberg, B. Walker, S. Gange, J. Gallant, and R. F. Siliciano.** 1999. Latent infection of CD4+ T cells provides a mechanism for lifelong persistence of HIV-1, even in patients on effective combination therapy. Nat. Med. **5:**512–517.
7. **Gartner, S., P. Markovits, D. M. Markovitz, M. H. Kaplan, R. C. Gallo, and M. Popovic.** 1986. The role of mononuclear phagocytes in HTLV-III/LAV infection. Science **233:**215–219.
8. **Garaci, E., S. Aquaro, C. Lapenta, A. Amendola, M. Spada, S. Covaceuszach, C. F. Perno, and F. Belardelli.** 2003. Anti-nerve growth factor Ab abrogates macrophage-mediated HIV-1 infection and depletion of CD4+ T lymphocytes in hu-SCID mice. Proc. Natl. Acad. Sci. USA **100:**8927–8932.
9. **Ichiyama, K., S. Yokoyama-Kumakura, Y. Tanaka, R. Tanaka, K. Hirose, K. Bannai, T. Edamatsu, M. Yanaka, Y. Niitani, N. Miyano-Kurosaki, H. Takaku, Y. Koyanagi, and N. Yamamoto.** 2003. A duodenally absorbable CXC chemokine receptor 4 antagonist, KRH-1636, exhibits a potent and selective anti-HIV-1 activity. Proc. Natl. Acad. Sci. USA **100:**4185–4190.
10. **Ito, M., H. Hiramatsu, K. Kobayashi, K. Suzue, M. Kawahata, K. Hioki, Y. Ueyama, Y. Koyanagi, K. Sugamura, K. Tsuji, T. Heike, and T. Nakahata.** 2002. NOD/SCID/γ(c)(null) mouse: an excellent recipient mouse model for engraftment of human cells. Blood **100:**3175–3182.
11. **Kavlick, M. F., and H. Mitsuya.** 2001. The emergence of drug resistant HIV-1 variants and its impact on antiretroviral therapy of HIV-1 infection, p. 279–312. *In* E. De Clercq (ed.), The art of antiretroviral therapy. American Society for Microbiology, Washington, D.C.
12. **Koh, Y., H. Nakata, K. Maeda, H. Ogata, G. Bilcer, T. Devasamudram, J. F. Kincaid, P. Boross, Y. F. Wang, Y. Tie, P. Volarath, L. Gaddis, R. W. Harrison, I. T. Weber, A. K. Ghosh, and H. Mitsuya.** 2003. Novel bis-tetrahydrofuranylurethane-containing nonpeptidic protease inhibitor (PI) UIC-94017 (TMC114) with potent activity against multi-PI-resistant human immunodeficiency virus in vitro. Antimicrob. Agents Chemother. **47:**3123–3129.
13. **Koyanagi, Y., S. Miles, R. T. Mitsuyasu, J. E. Merrill, H. V. Vinters, and I. S. Chen.** 1987. Dual infection of the central nervous system by AIDS viruses with distinct cellular tropisms. Science **236:**819–822.
14. **Koyanagi, Y., Y. Tanaka, J. Kira, M. Ito, K. Hioki, N. Misawa, Y. Kawano, K. Yamasaki, R. Tanaka, Y. Suzuki, Y. Ueyama, E. Terada, T. Tanaka, M. Miyasaka, T. Kobayashi, Y. Kumazawa, and N. Yamamoto.** 1997. Primary human immunodeficiency virus type 1 viremia and central nervous system invasion in a novel hu-PBL-immunodeficient mouse strain. J. Virol. **71:**2417–2424.
15. **Lee, B., M. Sharron, L. J. Montaner, D. Weissman, and R. W. Doms.** 1999. Quantification of CD4, CCR5, and CXCR4 levels on lymphocyte subsets, dendritic cells, and differentially conditioned monocyte-derived macrophages. Proc. Natl. Acad. Sci. USA **96:**5215–5220.
16. **Lyons, A. B.** 2000. Analysing cell division in vivo and in vitro using flow cytometric measurement of CFSE dye dilution. J. Immunol. Methods **243:**147–154.
17. **Maeda, K., K. Yoshimura, S. Shibayama, H. Habashita, H. Tada, K. Sagawa, T. Miyakawa, M. Aoki, D. Fukushima, and H. Mitsuya.** 2001. Novel low molecular weight spirodiketopiperazine derivatives potently inhibit R5

HIV-1 infection through their antagonistic effects on CCR5. J. Biol. Chem. **276:**35194–35200.
18. **Maeda, Y., M. Foda, S. Matsushita, and S. Harada.** 2000. Involvement of both the V2 and V3 regions of the CCR5-tropic human immunodeficiency virus type 1 envelope in reduced sensitivity to macrophage inflammatory protein 1α. J. Virol. **74:**1787–1793.
19. **McCune, J. M., R. Namikawa, C. C. Shih, L. Rabin, and H. Kaneshima.** 1990. Suppression of HIV infection in AZT-treated SCID-hu mice. Science **247:**564–566.
20. **Mitsuya, H., and S. Broder.** 1986. Inhibition of the in vitro infectivity and cytopathic effect of human T-lymphotropic virus type III/lymphadenopathy virus-associated virus (HTLV-III/LAV) by 2′,3′-dideoxynucleosides. Proc. Natl. Acad. Sci. USA **83:**1911–1915.
21. **Mitsuya, H., and S. Broder.** 1987. Strategies for antiviral therapy in AIDS. Nature **325:**773–778.
22. **Mitsuya, H., and J. Erickson.** 1999. Discovery and development of antiretroviral therapeutics for HIV infection, p. 751–780. *In* T. C. Merigan, J. G. Bartlet, and D. Bolognesi (ed.), Textbook of AIDS medicine. Williams & Wilkins, Baltimore, Md.
23. **Miura, Y., N. Misawa, Y. Kawano, H. Okada, Y. Inagaki, N. Yamamoto, M. Ito, H. Yagita, K. Okumura, H. Mizusawa, and Y. Koyanagi.** 2003. Tumor necrosis factor-related apoptosis-inducing ligand induces neuronal death in a murine model of HIV central nervous system infection. Proc. Natl. Acad. Sci. USA **100:**2777–2782.
24. **Miura, Y., N. Misawa, N. Maeda, Y. Inagaki, Y. Tanaka, M. Ito, N. Kayagaki, N. Yamamoto, H. Yagita, H. Mizusawa, and Y. Koyanagi.** 2001. Critical contribution of tumor necrosis factor-related apoptosis-inducing ligand (TRAIL) to apoptosis of human CD4+ T cells in HIV-1-infected hu-PBL-NOD-SCID mice. J. Exp. Med. **193:**651–660.
25. **Mosier, D. E., R. J. Gulizia, S. M. Baird, D. B. Wilson, D. H. Spector, and S. A. Spector.** 1991. Human immunodeficiency virus infection of human-PBL-SCID mice. Science **251:**791–794.
26. **Pan, G., J. Ni, Y. F. Wei, G. Yu, R. Gentz, and V. M. Dixit.** 1997. An antagonist decoy receptor and a death domain-containing receptor for TRAIL. Science **277:**815–818.
27. **Pan, G., K. O'Rourke, A. M. Chinnaiyan, R. Gentz, R. Ebner, J. Ni, and V. M. Dixit.** 1997. The receptor for the cytotoxic ligand TRAIL. Science **276:**111–113.
28. **Ratain, M., and W. Plunkett.** 1997. Pharmacology, p. 875–889. *In* J. Holland, R. Bast, Jr., D. Morton, E. Frei, D. KuFe, and R. Weichselbaum (ed.), Cancer medicine, 4th ed. Williams and Wilkins, Baltimore, Md.
29. **Ruxrungtham, K., E. Boone, H. Ford, Jr., J. S. Driscoll, R. T. Davey, Jr., and H. C. Lane.** 1996. Potent activity of 2′-β-fluoro-2′,3′-dideoxyadenosine against human immunodeficiency virus type 1 infection in hu-PBL-SCID mice. Antimicrob. Agents Chemother. **40:**2369–2374.
30. **Strizki, J. M., S. Xu, N. E. Wagner, L. Wojcik, J. Liu, Y. Hou, M. Endres, A. Palani, S. Shapiro, J. W. Clader, W. J. Greenlee, J. R. Tagat, S. McCombie, K. Cox, A. B. Fawzi, C. C. Chou, C. Pugliese-Sivo, L. Davies, M. E. Moreno, D. D. Ho, A. Trkola, C. A. Stoddart, J. P. Moore, G. R. Reyes, and B. M. Baroudy.** 2001. SCH-C (SCH 351125), an orally bioavailable, small molecule antagonist of the chemokine receptor CCR5, is a potent inhibitor of HIV-1 infection in vitro and in vivo. Proc. Natl. Acad. Sci. USA **98:**12718–12723.
31. **Walker, U. A., B. Setzer, and N. Venhoff.** 2002. Increased long-term mitochondrial toxicity in combinations of nucleoside analogue reverse-transcriptase inhibitors. AIDS **16:**2165–2173.
32. **Westervelt, P., H. E. Gendelman, and L. Ratner.** 1991. Identification of a determinant within the human immunodeficiency virus 1 surface envelope glycoprotein critical for productive infection of primary monocytes. Proc. Natl. Acad. Sci. USA **88:**3097–3101.
33. **Yahata, T., K. Ando, Y. Nakamura, Y. Ueyama, K. Shimamura, N. Tamaoki, S. Kato, and T. Hotta.** 2002. Functional human T lymphocyte development from cord blood CD34+ cells in nonobese diabetic/Shi-scid, IL-2 receptor gamma null mice. J. Immunol. **169:**204–209.
34. **Yoshida, A., R. Tanaka, T. Murakami, Y. Takahashi, Y. Koyanagi, M. Nakamura, M. Ito, N. Yamamoto, and Y. Tanaka.** 2003. Induction of protective immune responses against R5 human immunodeficiency virus type 1 (HIV-1) infection in hu-PBL-SCID mice by intrasplenic immunization with HIV-1-pulsed dendritic cells: possible involvement of a novel factor of human CD4(+) T-cell origin. J. Virol. **77:**8719–8728.
35. **Yoshimura, K., R. Kato, K. Yusa, M. F. Kavlick, V. Maroun, A. Nguyen, T. Mimoto, T. Ueno, M. Shintani, J. Falloon, H. Masur, H. Hayashi, J. Erickson, and H. Mitsuya.** 1999. JE-2147: a dipeptide protease inhibitor (PI) that potently inhibits multi-PI-resistant HIV-1. Proc. Natl. Acad. Sci. USA **96:**8675–8680.

THE JOURNAL OF BIOLOGICAL CHEMISTRY VOL. 281, NO. 2, pp. 1241–1250, January 13, 2006
Printed in the U.S.A.

Altered HIV-1 Gag Protein Interactions with Cyclophilin A (CypA) on the Acquisition of H219Q and H219P Substitutions in the CypA Binding Loop*

Received for publication, May 31, 2005, and in revised form, November 7, 2005 Published, JBC Papers in Press, November 7, 2005, DOI 10.1074/jbc.M505920200

Hiroyuki Gatanaga[‡1], Debananda Das[‡], Yasuhiro Suzuki[‡§], Damaris D. Yeh[‡], Khaja A. Hussain[¶], Arun K. Ghosh[¶], and Hiroaki Mitsuya[‡§2]

From the [‡]Experimental Retrovirology Section, HIV and AIDS Malignancy Branch, NCI, National Institutes of Health, Bethesda, Maryland 20892, the [§]Departments of Hematology and Infectious Diseases, Kumamoto University School of Medicine, Kumamoto 860, Japan, and the [¶]Department of Chemistry, University of Illinois, Chicago, Illinois 60607

HIV-1 Gag protein interaction with cyclophilin A (CypA) is critical for viral fitness. Among the amino acid substitutions identified in Gag noncleavage sites in HIV-1 variants resistant to protease inhibitors, H219Q (Gatanaga, H., Suzuki, Y., Tsang, H., Yoshimura, K., Kavlick, M. F., Nagashima, K., Gorelick, R. J., Mardy, S., Tang, C., Summers, M. F., and Mitsuya, H. (2002) *J. Biol. Chem.* 277, 5952–5961) and H219P substitutions in the viral CypA binding loop confer the greatest replication advantage to HIV-1. These substitutions represent polymorphic amino acid residues. We found that the replication advantage conferred by these substitutions was far greater in CypA-rich MT-2 and H9 cells than in Jurkat cells and peripheral blood mononuclear cells (PBM), both of which contained less CypA. High intracellular CypA content in H9 and MT-2 cells, resulting in excessive CypA levels in virions, limited wild-type HIV-1 (HIV-1_{WT}) replication and H219Q introduction into HIV-1 (HIV-1_{H219Q}), reduced CypA incorporation of HIV-1, and potentiated viral replication. H219Q introduction also restored the otherwise compromised replication of HIV-1_{P222A} in PBM, although the CypA content in HIV-$1_{H219Q/P222A}$ was comparable with that in HIV-1_{P222A}, suggesting that H219Q affected the conformation of the CypA-binding motif, rendering HIV-1 replicative in a low CypA environment. Structural modeling analyses revealed that although hydrogen bonds are lost with H219Q and H219P substitutions, no significant distortion of the CypA binding loop of Gag occurred. The loop conformation of HIV-1_{P222A} was found highly distorted, although H219Q introduction to HIV-1_{P222A} restored the conformation of the loop close to that of HIV-1_{WT}. The present data suggested that the effect of CypA on HIV-1 replicative ability is bimodal (both high and low CypA content limits HIV-1 replication), that the conformation of the CypA binding region of Gag is important for viral fitness, and that the function of CypA is to maintain the conformation.

Combination antiretroviral therapy has brought about improved quality of life and extended survival in patients with HIV-1[3] infection. However, the emergence of HIV-1 variants resistant to anti-HIV-1 therapeutic agents, including reverse transcriptase inhibitors and protease inhibitors (PIs), has limited the efficacy of chemotherapy (1). HIV-1 develops resistance mainly by substituting amino acids in the target viral enzyme or component; however, recent studies have revealed that certain polymorphic amino acid residues also contribute to the viral resistance (2, 3). We recently found that multiple amino acid substitutions emerged in noncleavage sites of the Gag protein, which were associated with the development of HIV-1 resistance against PIs (4). Among such amino acid substitutions, H219Q, occurring in the cyclophilin A (CypA) binding loop in the p24 Gag protein, conferred the greatest replication advantage on HIV-1 (4). CypA binds to p24 Gag protein, resulting in the packaging of ~200 copies of CypA into each HIV-1 virion (5, 6), and is thought to perform an essential role early in the HIV-1 replication cycle (7, 8), perhaps by destabilizing the capsid (p24 Gag protein) shell during viral entry and uncoating (9) and/or by performing an additional chaperon function, facilitating correct capsid condensation during viral maturation (10, 11).

In the present study, we asked how H219Q and H219P substitutions occurring within the viral CypA binding loop conferred replication advantage to HIV-1, and we examined whether these substitutions affected the conformation and interaction of p24 Gag protein and CypA during HIV-1 propagation in various host cells. We also attempted to better understand the functional role of CypA in HIV-1 replication. To that end, we determined the virological and biochemical properties of a variety of recombinant infectious clones and their CypA contents. We also carried out molecular modeling analyses of the wild-type and mutated p24 Gag complex with CypA. The data demonstrate that both H219Q and H219P enhance HIV-1 replication by reducing viral CypA contents in daughter virions as produced in CypA-rich cells, but not in cells that has a low CypA content. We suggest that the effect of CypA on HIV-1 replicative ability is bimodal, both high and low contents of CypA limit HIV-1 replication. The data also suggest that the conformation of p24 Gag is strongly correlated with viral fitness.

EXPERIMENTAL PROCEDURES

Antiviral Agents—Three PIs, KNI-272, JE-2147, and UIC-94003, were synthesized as described previously (12–16). Three newly synthesized PIs, UIC-00041, UIC-00142, and UIC-00145 (Fig. 1), were also

* This work was supported in part by the Intramural Research Program of the NCI, Center for Cancer Research, National Institutes of Health, in part by National Institutes of Health Grant GM 53386 (to A. K. G.), in part by Research for the Future Program Grant JSPS-RFTF 97L00705 from the Japan Society for the Promotion of Science (to H. M.), a grant-in-aid for scientific research (priority areas) from the Ministry of Education (to H. M.), a grant from the Culture, Sports, Sciences, and Technology of Japan (Monbu-Kagakusho) (to H. M.), and a grant for the promotion of AIDS research from the Ministry of Health Welfare and Labor of Japan (Kosei-Rohdosho) (to H. M.). The costs of publication of this article were defrayed in part by the payment of page charges. This article must therefore be hereby marked "*advertisement*" in accordance with 18 U.S.C. Section 1734 solely to indicate this fact.

[1] Present address: AIDS Clinical Center, International Medical Center of Japan, Tokyo 162-8655, Japan.

[2] To whom correspondence should be addressed: Experimental Retrovirology Section, HIV and AIDS Malignancy Branch, NCI, National Institutes of Health, Bldg. 10, Rm. 5A11, 9000 Rockville Pike, Bethesda, MD 20892. Tel.: 301-496-9238; Fax: 301-402-0709; E-mail: hmitsuya@helix.nih.gov.

[3] The abbreviations used are: HIV-1, human immunodeficiency virus, type 1; PBM, peripheral blood mononuclear cell; CHRA, competitive HIV-1 replication assay; CypA, cyclophilin A; PI, protease inhibitor; PHA, phytohemagglutinin; CsA, cyclosporin A; CA, capsid; WT, wild type.

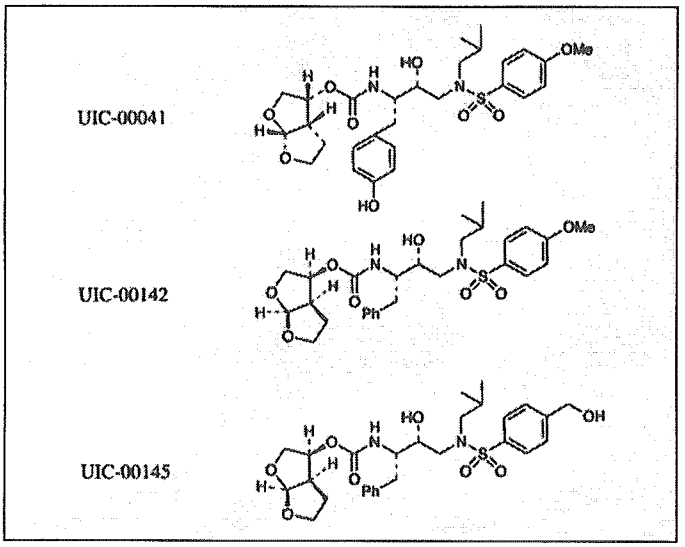

FIGURE 1. **Structures of UIC-00041, UIC-00142, and UIC-00145.**

synthesized by Ghosh and Hussain,[4] and the procedures for the synthesis will be published elsewhere.

Generation of HIV-1 Variants Resistant to PIs—The wild-type infectious clone, HIV-1_{WT}, produced by COS-7 cells transfected with pHIV-1_{NL4-3} was propagated in human $CD4^+$ MT-2 or H9 cells in the presence of increasing concentrations of an antiretroviral agent as described previously (4, 14, 16). Briefly, MT-2 or H9 cells (5×10^5) were exposed to wild-type HIV-1_{1NL4-3} and cultured in the presence of each PI at initial concentrations of 0.0005–0.03 μM. When the virus began to propagate in the presence of the drug, the drug concentration was increased. This selection was carried out for a total of 27–80 passages. For the generation of JE-2147-resistant virus, an infectious clone carrying I84V substitution in the protease (HIV-1_{I84V}) was employed instead of HIV-1_{WT} (14). Proviral DNA in the lysates of HIV-1-infected cells of the last passage was sequenced as indicated (4).

Generation of Recombinant HIV-1 Clones—To generate HIV-1 clones carrying the desired mutations, the site-directed mutagenesis was performed, and the mutation-containing genomic fragments thus obtained were introduced to pHIV-1_{NLSma} as described previously (4). An infectious clone containing P222A mutation in Gag was generated using a plasmid kindly provided by Drs. D. Braaten and J. Luban (5). Each recombinant plasmid was transfected into COS-7 cells, and the obtained infectious virions were harvested 48 h after transfection and stored at −80 °C until use (4).

Replication Kinetic Assay—MT-2, H9, Jurkat cells (10^5), or phytohemagglutinin-stimulated peripheral blood mononuclear cells (PHA-PBM: 5×10^6) were exposed to each infectious virus preparation (500 blue-cell-forming units defined in the MAGI assay) (17) for 12 h, washed twice with phosphate-buffered saline, and cultured in 5 ml of complete medium in the presence or absence of cyclosporin A (CsA). Culture supernatants (200 μl) were harvested every other day or every 4 days, and p24 Gag amounts were determined using a commercially available radioimmunoassay kit (PerkinElmer Life Sciences). An enzyme-linked immunosorbent assay kit (Beckman Instruments, Fullerton, CA) was also used for the determination of p24 Gag amounts as needed.

Competitive HIV-1 Replication Assay Using PHA-PBM—In order to compare the replication rates of infectious HIV-1 clones, the competitive HIV-1 replication assay (CHRA) was performed as described previously (18) with some modifications. In brief, PHA-PBMs (5×10^6) were exposed to various mixtures of the paired infectious clones to be examined for their replicative ability and were cultured for the indicated times. Every 7 days, the supernatants of the virus co-culture were transferred to freshly prepared uninfected PHA-PBM cultures. DNA purified from the cells harvested at each passage was subjected to direct DNA sequencing of the HIV-1 genome, and viral population changes were evaluated based on relative peak heights in the electropherogram (18).

Western Blot Analysis—For the analysis of cellular CypA contents, MT-2 cells, H9 cells, Jurkat cells, or PHA-PBMs were lysed with lysis buffer (4), and the amounts of lysates were normalized with cell numbers or total protein contents using a bicinchoninic acid protein assay kit (Pierce). For the analysis of virion-associated CypA, the culture supernatants of chronically HIV-1-infected H9 or Jurkat cells were centrifuged and passed through a 0.22-μm pore-size filter to remove cellular debris; the filtrates were normalized with p24 contents measured with radioimmunoassay and were ultracentrifuged to pellet virions (4). The pelleted virions were lysed in lysis buffer. The resultant samples were processed with SDS-polyacrylamide gradient gels, and CypA was visualized by SuperSignalWestPico (Pierce) using anti-CypA antiserum (Biomol, Plymouth Meeting, PA). An anti-p24 Gag antiserum (Advanced Biotechnologies, Inc., Columbia, MD) served as a control to ensure that appropriate amounts of the samples were loaded. The signal density of CypA and p24 Gag was analyzed on a Windows computer by using the ImageJ Program (developed at National Institutes of Health, rsb.info.nih.gov/ij/) as published previously (19).

Molecular Modeling of the $p24_{CA151}$-CypA Complex with p24 Amino Acid Substitutions—The crystal structure of human CypA that was bound to the amino-terminal domain of p24 Gag (capsid residues 1–151 (CA_{151}), Protein Data Bank code 1AK4) (9) was analyzed to determine the changes with H219Q or H219P substitution. There were two CA-CypA complexes in the structure. Chain A of CypA and chain D of CA form one complex and were retained for the calculation. Identical results should be obtained with the other complex (chain B of CypA and chain C of CA) because the conformations of both CypA and CA in these complexes are quite similar. Structural modifications, visualization, and analysis were performed utilizing the Maestro interface from Schrödinger (Maestro 7.0, Schrödinger, LLC, New York). OPLS2003 force field (20) as implemented in MacroModel 9.0 (MacroModel, version 9.0, Schrödinger, LLC, New York) was used for minimizing mutated structures and for carrying out molecular dynamics calculations. OPLS2003 uses an enhanced version of the widely used OPLS-AA force field and has improved parameters for peptides. It was verified that the force field had high quality bond stretching, bending, and torsional parameters. Charges were taken from the force field. Molecular dynamics calculations were carried out on the wild-type complex and on the mutated structures. The structures were initially minimized for 2500 iterations. A constant temperature of 300 K and SHAKE constraints for bonds to hydrogens were used. The GB/SA continuum solvation model, with water as the solvent, was used (21). While calculating nonbonded interactions, cut-off distances of 8 and 20 Å were used for van der Waals and electrostatic interactions, respectively. Using a time step of 2 fs, the structures were equilibrated for 20 ps, and the simulation was carried out for 1 ns. Structures were monitored at intervals of every 50 ps. Calculations were carried out on an SGI Origin 3400 computer platform. For the wild type and for each mutant structure, 1-ns molecular dynamics calculation takes about 11 days under the stated conditions on this high performance computational platform.

[4] A. K. Ghosh and K. A. Hussain, personal communication.

TABLE 1

Amino acid substitutions identified in the protease and p24 Gag protein of HIV-1 variants selected against PI

Amino acid substitutions listed are based on the amino acid sequences deduced from the nucleotide sequence of the protease-encoding and the entire Gag-encoding genes of each HIV-1 selected against an indicated PI.

PI	Strain	Cell	Passage	Amino acid substitutions identified in	
				Protease	p24
KNI-272	HIV-1_{NL4-3}[a]	MT-2	27	V32I/M46I/V82I/I84V	H219Q
KNI-272	HIV-1_{LAI}	H9	55	V32I/L33F/K45I/F53L/A71V/I84V	H219Q
APV	HIV-1_{NL4-3}[a]	MT-2	31	L10F/V32I/M46I/I54M/A71V/I84V	H219Q
JE-2147	HIV-$1_{NL4-3/I84V}$[a]	MT-2	33	M46I/I47V/V82I/I84V	H219Q
UIC-94003	HIV-1_{NL4-3}[a]	MT-2	62	L10F/A28S/M46I/I50V/A71V	Q199H/H219Q
UIC-00041	HIV-1_{NL4-3}	MT-2	73	K43I/L63P/V82I	M200I/H219P
UIC-00142	HIV-1_{NL4-3}	MT-2	84	L10F/V32I/M46I/I84V	H219Q
UIC-00145	HIV-1_{NL4-3}	MT-2	80	L10F/V32I/M46I/I47A/K55N	H219Q

[a] PI-resistant HIV-1 variants described previously (4) are shown.

RESULTS

Amino Acid Substitutions Identified in p24 Gag Protein in HIV-1 Variants Resistant to PI—We have reported previously that several amino acid substitutions were seen in common in the Gag protein at noncleavage sites among HIV-1 variants that acquired *in vitro* a high multitude of resistance to PIs such as APV, JE-2147, KNI-272, and UIC-94003 (4). In an attempt to corroborate and extend our previous observations and to determine how often such amino acid substitutions develop in the Gag protein, we examined four more HIV-1 variants that were selected *in vitro* against various PIs, including three novel PIs, UIC-00041, UIC-00142, and UIC-00145. Table 1 depicts the properties of eight PI-resistant HIV-1 variants (including four HIV-1 variants reported previously). Seven of the eight variants were selected against PIs in MT-2 cells, although one variant was selected in H9 cells. The strains used were HIV-1_{1NL4-3} and HIV-1_{LAI}, and 3–6-amino acid substitutions were identified in the protease. It was noted that all eight variants had in common an amino acid substitution at position 219 in p24 Gag protein, seven variants had H219Q substitution and one had H219P substitution. The His^{219} residue is located within the CypA binding loop and is thought to play a role in the p24 Gag interactions with CypA through a hydrogen bond and hydrophobic contact(s) (9). It is worth noting that when HIV-1_{1NL4-3} was propagated in the absence of PI in MT-2 cells, the virus also acquired H219Q, V218M, or A224V mutation by passage 10 (4). It should be noted that two amino acids, Val^{218} and Ala^{224}, are also located within the CypA binding loop of the p24 Gag protein and are also known to interact with CypA through hydrophobic contacts (9). These data, taken together, strongly suggest that the amino acids interacting with CypA, in particular His^{219}, are prone to undergo substitutions under certain circumstances and are associated with viral replication fitness. Indeed, in the HIV Sequence Compendium 2000 (22), of 88 different HIV-1 strains, 65 had histidine at the position 219, whereas 13 had glutamine, and 4 had proline at the position 219, indicating that both Gln^{219} and Pro^{219} represent polymorphic amino acid residues. Hence, the present data suggest that these two polymorphic amino acids are associated with viral fitness and possibly to the acquisition of resistance to certain PIs.

Effects of Gag Mutations at Position 219 on HIV-1 Replication—In order to examine the effects of the Gag mutation at position 219 on HIV-1 replication, we generated two infectious HIV-1 clones, HIV-1_{H219Q} and HIV-1_{H219P}, and we assessed their virologic properties. In MT-2 cells, HIV-1_{H219Q} rapidly replicated compared with the wild-type HIV-$1_{WT(His-219)}$ (Fig. 2*A*), in agreement with our previous observation (4). HIV-1_{H219Q} also replicated more rapidly than HIV-1_{WT} in H9 cells (Fig. 2*B*). HIV-1_{H219P} replicated as rapidly as HIV-1_{H219Q}, suggesting that the amino acid at position 219 is critical for the replication fitness of HIV-1. When we examined the fitness of the three infectious clones (HIV-1_{WT}, HIV-1_{H219Q}, and HIV-1_{H219P}) in $CD4^+$ Jurkat cells and PHA-PBM, there was no significant difference seen in their replication fitness (Fig. 2, *C* and *D*).

Competitive HIV-1 Replication Assays for H219Q Mutation in PHA-PBM—As shown above, although HIV-1_{H219Q} exhibited a greater replication capability when propagated in MT-2 and H9 cells compared with HIV-1_{WT}, there was no apparent difference in the replication profiles of HIV-1_{H219Q} and HIV-1_{WT} as propagated in PHA-PBM (Fig. 2, *A*, *B* and *D*). In order to evaluate the possible biological relevance of the replication kinetic data generated by using immortalized and long term cultured MT-2 and H9 cells, we conducted a modified competitive HIV-1 replication assay (CHRA) (18), in which freshly prepared PHA-PBM served as host cells. HIV-1_{H219Q} readily and uniformly overgrew HIV-1_{WT} in CHRA regardless of three different ratios of paired clones used in the assay (Fig. 2, *E–G*). These data indicated that the H219Q substitution conferred replication advantages on HIV-1 when propagated in immortalized $CD4^+$ T cells as well as PHA-PBM. It should be noted, however, that the replication advantage of HIV-1 acquired with the H219Q substitution was limited in PHA-PBM and was detected only when assessed with CHRA.

MT-2 and H9 Cells Contain Greater Amounts of CypA—The Gag mutations H219Q and H219P conferred significant replication advantage on HIV-1 as propagated in MT-2 cells and H9 cells, but such advantage was limited in PHA-PBM. Considering that His^{219} is located within the CypA binding loop and that HIV-1 replication is known to be affected by intracellular CypA contents (6, 7), we examined intracellular CypA content in each cell preparation by using Western blot analysis. As shown in Fig. 3, *A* and *B*, the CypA contents in 10^4 MT-2 (relative density, 100%) and 10^4 H9 cells (79.6%) appeared to be greater than those in 5×10^4 Jurkat cells (55.4%) and 5×10^4 PHA-PBM (42.9%), suggesting that MT-2 and H9 cells contained 6–12 times as much CypA per cell as Jurkat cells and PHA-PBM. As normalized with total cellular protein amounts, the CypA content in 1 μg of MT-2 and H9 cellular protein preparations was comparable with that in 2–4 μg of Jurkat protein preparations and that in 4 μg of PHA-PBM protein, suggesting that the former two cell preparations contained 2–4-fold greater amounts of CypA per cellular protein than the latter two cell preparations. These data showed that MT-2 and H9 cells have greater CypA amounts than Jurkat T cells and PHA-PBM.

Decreased CypA Incorporation into HIV-1_{H219Q} Virions—Considering that the data from crystal structure analyses by Gamble *et al.* (9) of p24 Gag protein complexed with CypA showing that His^{219} binds to Asn^{71} and Gln^{111} of CypA through a hydrogen bond and hydrophobic contact(s), respectively, we postulated that H219Q and H219P substitutions cancel or weaken such hydrogen bonds, resulting in the reduction of p24 binding to CypA and of CypA incorporation into daughter virions, leading to increased HIV-1 replication in CypA-rich MT-2 and H9 cells. We then examined the virion-associated CypA amounts in

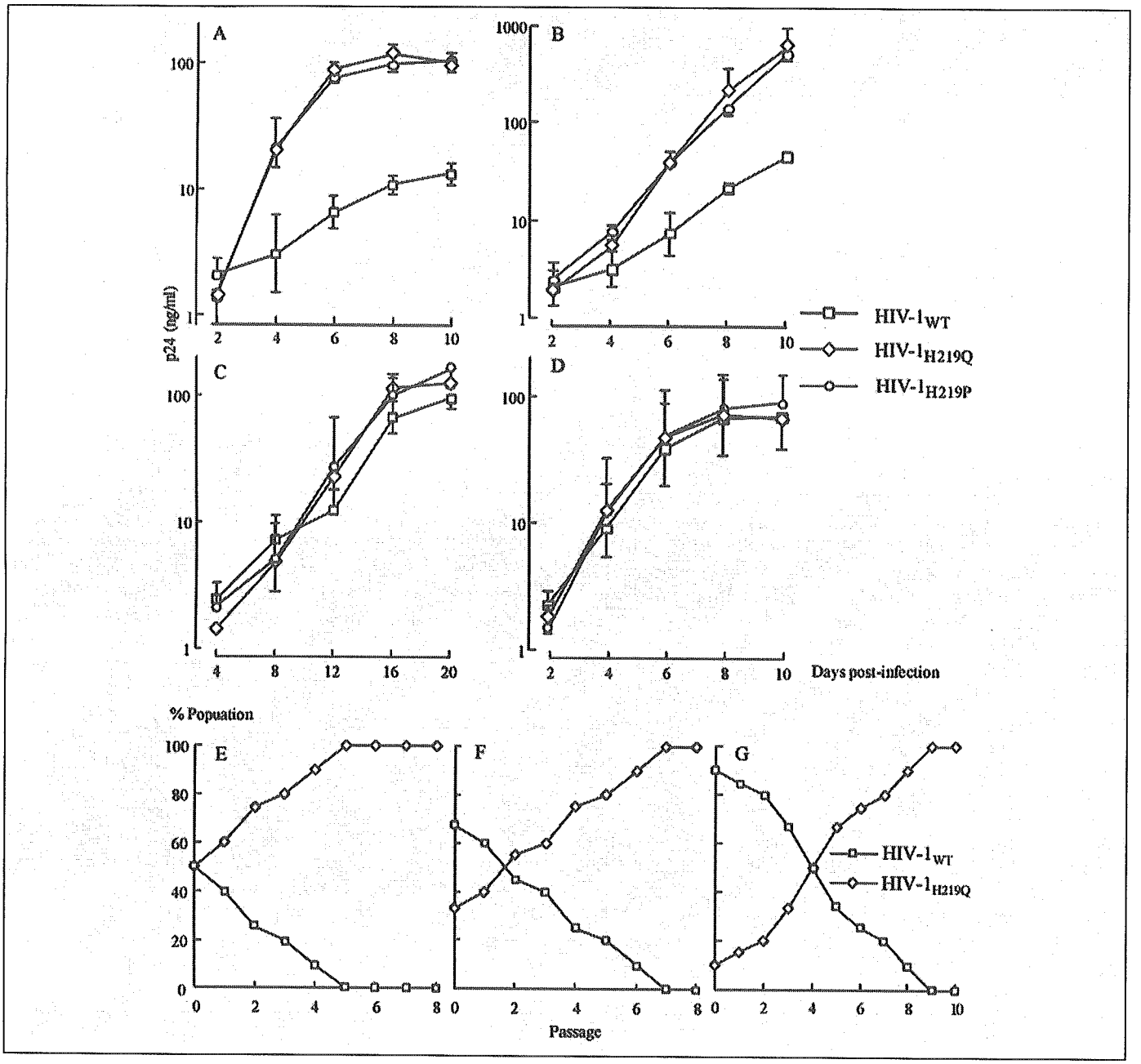

FIGURE 2. **Replication kinetics of HIV-1_{WT}, HIV-1_{H219Q}, and HIV-1_{H219P}.** MT-2 cells, H9 cells, Jurkat cells, and PHA-PBM (*A–D*, respectively) were exposed to each HIV-1 clone and cultured for the indicated numbers of passage. Virus replication was monitored by measuring the amounts of p24 Gag protein produced in the culture supernatants. The data shown represent geometric means (± 1 S.D.) of three independent experiments. Replication profiles of HIV-1_{WT} and HIV-1_{H219Q} in PHA-PBM were examined using CHRA (*E–G*). Two infectious HIV-1 clones to be compared for their fitness were mixed and propagated in PHA-PBM. The cell-free supernatant was transferred to fresh PHA-PBM every 7 days. The ratios of HIV-1_{WT} and HIV-1_{H219Q} at the initiation of the assay were 50:50, 67:33, and 90:10 (*E–G*, respectively). High molecular weight DNA extracted from infected cells at the end of each passage was subjected to nucleotide sequencing, and the proportions of His and Gln at position 219 in Gag protein were determined.

three infectious HIV-1 clones containing HIV-1_{WT}, HIV-1_{H219Q}, and HIV-1_{H219P}, employing Western blotting analysis using anti-p24 Gag and anti-CypA antisera. The culture supernatants of chronically HIV-1-infected H9 cells were prepared to contain the same amount of p24. The virions in each supernatant thus prepared were pelleted by ultracentrifugation and subsequently subjected to SDS-PAGE. Direct sequencing of cellular DNA confirmed that no unintended mutations developed during the culture. As shown in Fig. 3*C-1–3*, the experiment was performed three times. Percent densities of the CypA signal relative to each p24 Gag signal (making each signal 100%) were 11.1, 7.38, and 6.01% (Fig. 3*C-1*); 6.99, 4.99, and 4.71% (Fig. 3*C-2*), and 18.1, 12.0, and 11.2% (Fig. 3*C-3*) for HIV-1_{WT}/H9, HIV-1_{H219Q}/H9, and HIV-1_{H219P}/H9, respectively. These data demonstrated that H219Q and H219P substitutions increased HIV-1 replication in CypA-rich cells, which was associated with the substantial reduction of CypA incorporation into daughter virions.

p24 Gag Binding to CypA Affects HIV-1 Replication Kinetics—Yin *et al.* (23) have reported that the addition of CsA (0.5 μM) reduces CypA incorporation into daughter virions and increases replication rates of HIV-1_{1NL4-3} in H9 cells, suggesting that excessively high intracellular CypA contents may reduce HIV-1 replication rates. We then examined the effects of CsA on the replication rates of HIV-1_{WT} (Fig. 4, *A–D*) and HIV-1_{H219Q} (Fig. 4, *E–H*) in four different cell preparations.

In MT-2 and H9 cells, 0.5 μM CsA increased the replication rate of HIV-1_{WT}, whereas at a higher concentration (2.5 μM) its replication rate

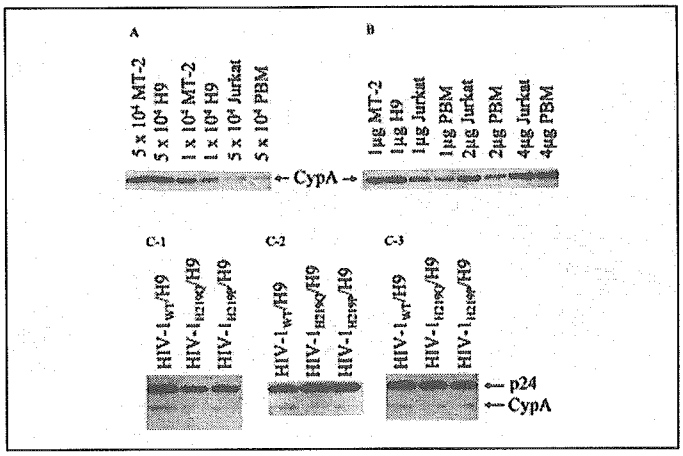

FIGURE 3. **MT-2 and H9 cells contain greater amounts of CypA than Jurkat cells and PHA-PBM, and HIV-1_{H219Q} and HIV-1_{H219P} virions contain reduced amounts of CypA than HIV-1_{WT} virions.** MT-2 cells, H9 cells, Jurkat cells, and PHA-PBM were lysed with lysis buffer, and the samples loaded were normalized by cell numbers or total protein contents. CypA was visualized with Western blotting analysis using anti-CypA antiserum (*A* and *B*). Percent CypA signal densities in 5×10^4 MT-2 cells, 5×10^4 H9 cells, 1×10^4 H9 cells, 5×10^4 Jurkat cells, and 5×10^4 PHA-PBM were 340.1, 387.4, 79.6, 55.4, and 42.9%, respectively, as compared with that in 1×10^4 MT-2 cells (serving as a standard to be 100%) (*A*). Percent CypA signal densities in 1 μg of H9 cells, 1 μg of Jurkat cells, 1 μg of PBM, 2 μg of Jurkat cells, 2 μg of PBMs, 4 μg of Jurkat cells, and 4 μg of PBMs were 155.2, 70.6, 35.0, 131.1, 59.5, 258.3, and 126.0%, respectively, as compared with that in 1 μg of MT-2 cells (serving as a standard to be 100%) (*B*). HIV-1 virions in the culture supernatants of chronically HIV-1-infected H9 cells were pelleted and subjected to Western blotting analysis for the determination of virion-associated CypA amounts using anti-p24 Gag and anti-CypA antisera. This experiment was performed three times (*C-1–3*). Percent densities of the CypA signal relative to each p24 Gag signal (making each p24 signal 100%) were 11.1, 7.38, and 6.01% in *C-1*; 6.99, 4.99, and 4.71% in *C-2*; and 18.1, 12.0, and 11.2% in *C-3* for HIV-1_{WT}/H9, HIV-1_{H219Q}/H9, and HIV-1_{H219P}/H9, respectively.

was reduced (Fig. 4, *A* and *B*), in agreement with the data by Yin *et al.* (23). In contrast, in Jurkat cells no increase in replication rate was seen, but rather CsA decreased HIV-1_{WT} replication in a dose-dependent manner (Fig. 4*C*). In PHA-PBM, CsA significantly decreased the replication rate of HIV-1_{WT}, and with 2.5 and 10 μM CsA, HIV-1_{WT} only poorly replicated (Fig. 4*D*). These data suggest that CsA (0.5 μM) can potentiate HIV-1_{WT} replication only in CypA-rich host cells. We further examined the effects of CsA on the replication of HIV-1_{H219Q} under the same conditions. In MT-2 and H9 cells (Fig. 4, *E* and *F*), no replication enhancement was seen with CsA added, but rather a reduced replication rate was observed in the presence of 0.5, 2.5, and 10 μM CsA. In Jurkat cells and PHA-PBM, the addition of CsA reduced the replication rate of HIV-1_{H219Q} as seen with HIV-1_{WT} (Fig. 4, *G* and *H*).

Taken together, the data suggest that the high intracellular CypA content in MT-2 and H9 cells was prohibitive to the replication of HIV-1_{WT} and that an appropriate concentration of CsA enhanced HIV-1_{WT} replication in CypA-rich cells by reduction of CypA incorporation into virions. In case of HIV-1_{H219Q}, however, H219Q already had reduced CypA incorporation into virions, and no enhanced replication was seen even in CypA-rich cells.

Effects of H219Q and P222A Substitutions on HIV-1 Replication—An amino acid substitution at position 222 from Pro to Ala (P222A) has been shown to substantially decrease the binding of p24 Gag protein to CypA and the CypA incorporation into daughter virions, causing reduced HIV-1 replication in Jurkat cells (6). As shown in Fig. 5, *A* and *B*, as examined in MT-2 and H9 cells, HIV-1_{NL4-3} carrying P222A (HIV-1_{P222A}) had a relatively low replication rate compared with HIV-1_{WT} in both host cells. However, with the introduction of both H219Q and P222A substitutions, HIV-$1_{H219Q/P222A}$ acquired faster replication rate; it replicated more rapidly than HIV-1_{WT} in MT-2 cells and comparably in H9 cells. In contrast, as examined in Jurkat cells, HIV-1_{P222A} showed a substantially decreased replication rate (Fig. 5*C*). In PHA-PBM, HIV-1_{P222A} was virtually replication-incompetent (Fig. 5*D*). As expected, with the H219Q substitution added, HIV-$1_{H219Q/P222A}$ exhibited an improved replication rate, which, however, yet remained below that of HIV-1_{WT} both in Jurkat cells and PHA-PBM (Fig. 5, *C* and *D*).

These data suggested either that the added H219Q substitution enabled HIV-1_{P222A} to incorporate more CypA into daughter virions or that H219Q altered or restored a conformation of the CypA binding domain of p24 Gag protein, thereby rendering the virus replication-competent without increasing CypA content.

H219Q Substitution Improves HIV-1_{P222A} Fitness without Increasing CypA Content—In order to ask whether H219Q improved the otherwise compromised CypA incorporation caused by the P222A substitution into virions or H219Q rendered HIV-1_{P222A} replication-competent without increasing CypA content, we examined the virion-associated CypA amounts by employing Western blotting analysis.

As can be seen in Fig. 5*E-1–3*, as HIV-1 virions in the culture supernatants of chronically HIV-1-infected H9 or Jurkat cells were pelleted and subjected to Western blotting analysis for the determination of virion-associated CypA amounts using anti-p24 Gag and anti-CypA antisera, the percent densities of the CypA signal relative to each p24 Gag signal (making each p24 signal 100%) were 33.8, 8.03, 6.92, and 6.48% in Fig. 5*E-1*; 26.3, 14.1, 6.93, and 6.19% in Fig. 5*E-2*; and 16.8, 6.48, 5.72, and 5.51% in Fig. 5*E-3* for HIV-1_{WT}/H9, HIV-1_{WT}/Jurkat, HIV-1_{P222A}/H9, and HIV-$1_{H219Q/P222A}$/H9, respectively, although HIV-$1_{H219Q/P222A}$ had a greater replication rate compared with HIV-1_{P222A} (Fig. 5, *A–E*).

These data demonstrated that HIV-1_{WT} produced by Jurkat cells and HIV-1_{P222A} produced by H9 cells contained approximately less than half and approximately one-fourth of the CypA amount detected in HIV-1_{WT} produced by H9 cells, respectively. The data strongly suggested that H219Q altered the conformation of the CypA binding domain of p24 Gag protein without affecting the CypA incorporation into HIV-1_{P222A} virions, thus rendering HIV-1_{P222A} replication relatively independent of CypA. It is possible that H219Q substitution not only decreased the incorporation of CypA into HIV-1 but also altered the conformation of Gag protein, thus leading to increased HIV-1 replication especially when HIV-1 is produced in CypA-rich cells. The latter effect of H219Q substitution is apparently viable in the presence of P222A substitution because increased HIV-$1_{H219Q/P222A}$ replication was seen without significant changes in CypA content in virions (Fig. 5, *A–E*).

Molecular Modeling of the p24 Gag CA_{151}-CypA Complex with H219Q or H219P—We finally carried out molecular modeling studies to better understand the following two aspects: the reason for less viral incorporation of CypA with H219Q, H219P, and P222A substitutions, and the rescue of viral replication with the H219Q/P222A double mutation. The crystal structure determined by Gamble *et al.* (9) revealed the sequence-specific interactions of p24 Gag (CA_{151}) with CypA (Fig. 6*A*). Those interactions include seven hydrogen bonds between residues 219 and 223 (excluding the bonds mediated through bridging water molecules) and various hydrophobic contacts, all of which appear to stabilize the interactions between p24 Gag and CypA (Fig. 6*B*). Our molecular dynamics calculations for 1 ns show valuable insights to the changes in interaction between wild-type and mutated p24 Gag and CypA. Initially, the change in conformation of the wild-type structure as well as the fluctuation of the hydrogen bonds between CA and CypA at intervals of 50 ps up to 1 ns was analyzed. The backbone conformation essentially remains the same even though there is loss of the hydrogen bonds between His^{219} and $Asn^{71}{}_{CypA}$ during this dynamics calculation. The

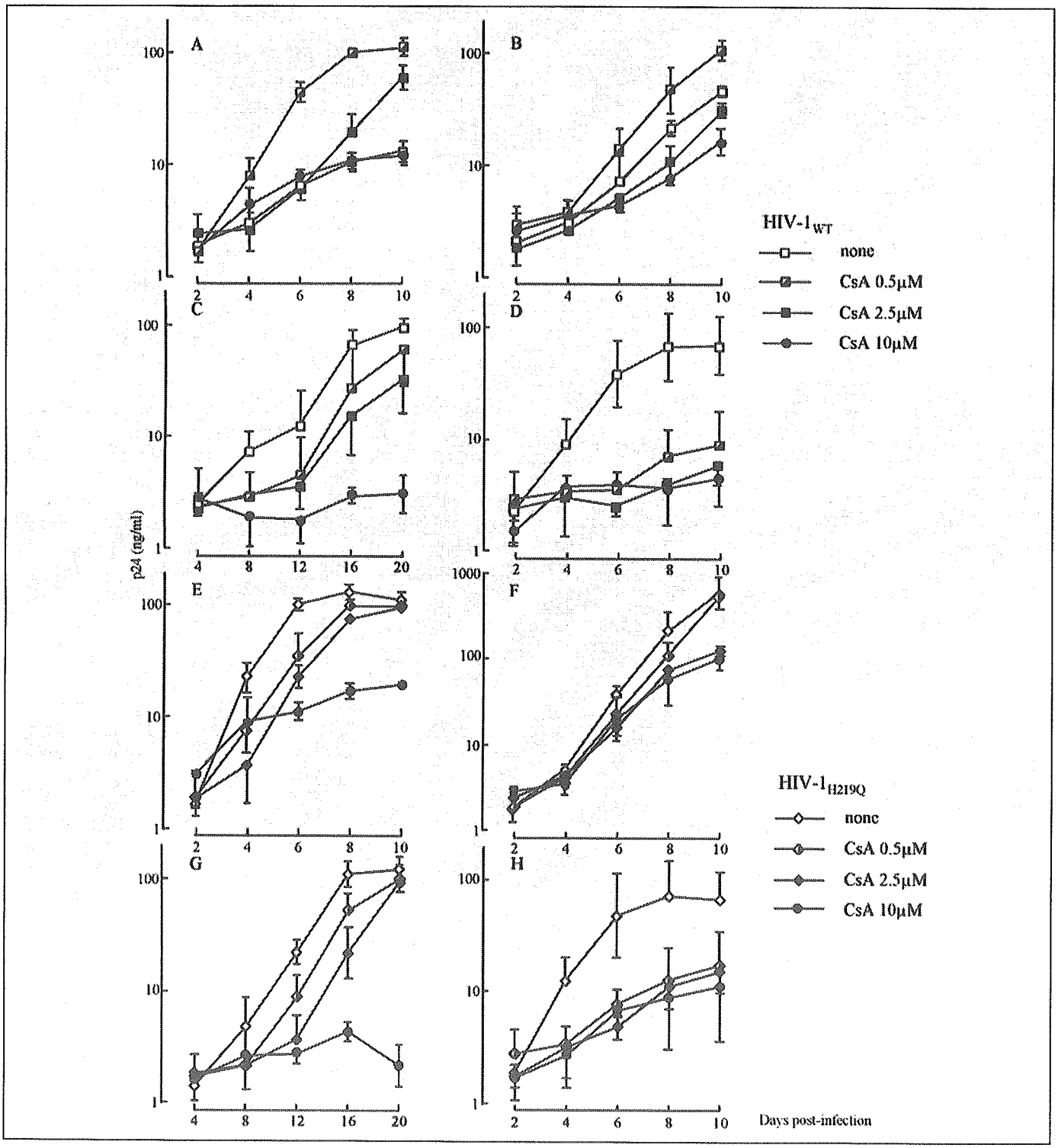

FIGURE 4. **Effects of CsA on HIV-1_{WT} and HIV-1_{H219Q} replication in various cell cultures.** MT-2 cells, H9 cells, Jurkat cells, and PHA-PBMs (*A–D*, respectively) were exposed to HIV-1_{WT} and cultured in the presence or absence of 0.5, 2.5, or 10 μM CsA. MT-2 cells, H9 cells, Jurkat cells, and PHA-PBMs (*E–H*, respectively) were also exposed to HIV-1_{H219Q} and cultured in the presence or absence of 0.5, 2.5, or 10 μM CsA. Virus replication was monitored with the amounts of p24 produced in the culture supernatants. The data shown represent geometric means (± 1 S.D.) of three independent experiments.

hydrogen bonds between Pro^{222} and $Arg^{55}{}_{CypA}$, Gly^{221}–$Asn^{102}{}_{CypA}$, and Ala^{220}–$Gln^{63}{}_{CypA}$ are the most invariant. Theses data suggest that the backbone conformation of the CypA binding region of p24 Gag is maintained with the mutation at position 219. For the mutated structures, the loop conformations at the end of 1 ns of molecular dynamics calculation were compared with the wild-type crystal structure. The weighted root mean square differences of the structures were calculated after a best fit of residues from Val^{218} to Ala^{224}. The root mean square differences of CA_{H219Q} from the wild-type CA_{151} was only 0.99 Å. Even though there is loss of hydrogen bond interactions with H219Q substitution, the loop conformations that depend on the overall conformational contact between CA and CypA do not undergo significant change (Fig. 6, *C* and *D*). The loss of the hydrogen bond between residue 219 of CA and CypA reduces the strong interaction between CA and CypA

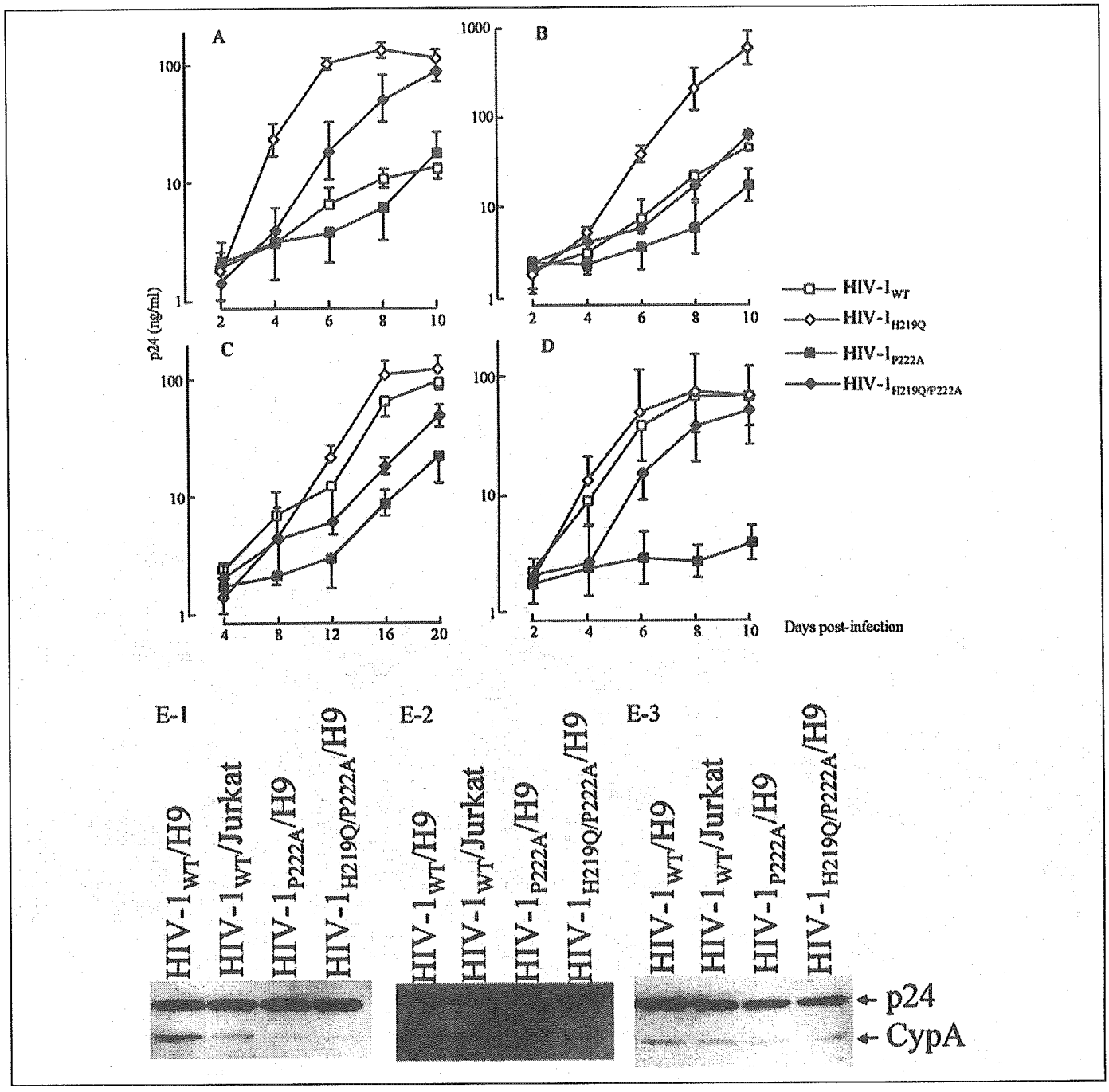

FIGURE 5. **Replication kinetics of HIV-1_{WT}, HIV-1_{H219Q}, HIV-1_{P222A}, and HIV-$1_{H219Q/P222A}$ and virion-associated CypA amounts in various HIV-1 preparations.** MT-2 cells, H9 cells, Jurkat cells, and PHA-PBMs (*A–D*, respectively) were exposed to each HIV-1 clone and cultured. Virus replication was monitored with the amount of p24 produced in the culture supernatants. The data shown represent geometric means (± 1 S.D.) of three independent experiments. HIV-1 virions in the culture supernatants of chronically HIV-1-infected H9 or Jurkat cells were pelleted and subjected to Western blotting analysis for the determination of virion-associated CypA amounts using anti-p24 Gag and anti-CypA antisera. This experiment was performed three times (*E-1–3*). Percent densities of the CypA signal relative to each p24 Gag signal (making each p24 signal 100%) were 33.8, 8.03, 6.92, and 6.48% in *E-1*; 26.3, 14.1, 6.93, and 6.19% in *E-2*; and 16.8, 6.48, 5.72, and 5.51% in *E-3* for HIV-1_{WT}/H9, HIV-1_{WT}/Jurkat, HIV-1_{P222A}/H9, and HIV-$1_{H219Q/P222A}$/H9, respectively.

and in a CypA-rich environment helps in improving viral replication. As shown in Fig. 7*A*, in the ribbon diagram of CA_{P222A} superimposed on that of CA_{WT}, CA_{P222A} causes a significant distortion of the loop structure. The value of weighted root mean square deviation of the structure of CA_{P222A} from CA_{WT} structure is 3.16 Å. In comparison, as can be seen in the ribbon diagrams of the structures of the CypA binding region of various mutant CA species (Fig. 7*B*), generated with 1-ns dynamics calculations and superimposed on the structure of CA_{WT}, H219Q and H219P substitutions do not significantly affect the conformation of the CypA binding region of CA_{WT}.

Effects of H219Q and P222A Substitutions on the Conformation of the CypA Binding Loop—It is of note that P222A not only results in less CypA incorporation but the significant change in loop conformation is probably responsible for reduction in viral replication. That the loop conformation is responsible for viral fitness is further evidenced by analysis of the structures with concurrent H219Q and P222A substitutions. These two concurrent substitutions recovered the distortion of the loop conformation that was associated with P222A mutation alone (Fig. 7*A*). Fig. 7*B* illustrates that the conformations of the CypA binding region of CA_{WT} and mutant CA species structurally resemble each other. The

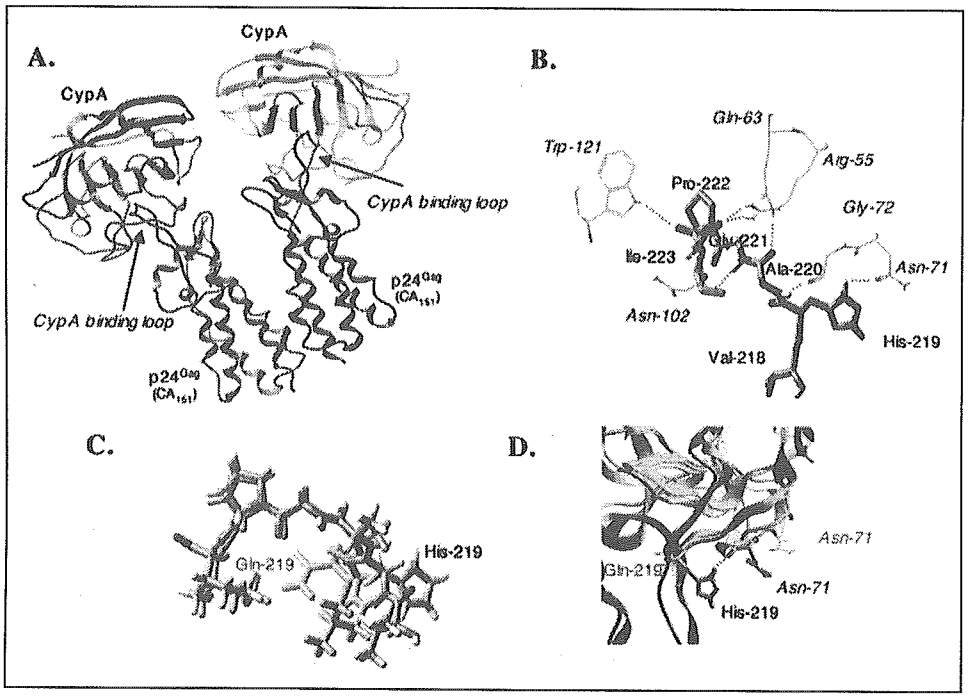

FIGURE 6. **Loss of hydrogen bonds in CA_{151}-CypA complex with H219Q or H219P substitution.** *A*, there are two p24 Gag CA_{151}-CypA complexes in the asymmetric unit (9). *B*, in the area of the CypA binding loop shown there are seven hydrogen bonds, which are between His^{219}–$Asn^{71}{}_{CypA}$, Ala^{220}–$Gln^{63}{}_{CypA}$, Ala^{220}–$Gly^{72}{}_{CypA}$, Gly^{221}–$Asn^{102}{}_{CypA}$, Pro^{222}–$Arg^{55}{}_{CypA}$ (two hydrogen bonds), and Ile^{223}–$Trp^{121}{}_{CypA}$. These hydrogen bonds along with hydrophobic contacts are responsible for maintaining the optimum relative conformations of p24 and CypA. *C*, H219Q substitution results in the loss of the following three hydrogen bond interactions: Gln^{219}–$Asn^{71}{}_{CypA}$, Ala^{220}–$Gly^{72}{}_{CypA}$, and Ile^{223}–$Trp^{121}{}_{CypA}$ and causes a significant conformational change of the contact region of the CypA binding loop (see *D*). *D*, changes in the complex configurations with H219Q substitution. Note that in the mutated structure Gln^{219} (*wire*) is located far apart from $Asn^{71}{}_{CypA}$ (*wire*), although in the wild-type structure His^{219} (*stick*) forms a tight hydrogen bond with $Asn^{71}{}_{CypA}$ (*stick*). CA_{WT} is shown by a *green ribbon* and the complexed CypA by a *yellow ribbon*; CA_{H219Q} is shown by a *red tube* and the complexed CypA by a *pink tube*. The loss of hydrogen bonds results in reduced CypA incorporation, but there persists sufficient interaction so that there are minimal alterations in the conformation of the CypA binding loop of CA_{151}.

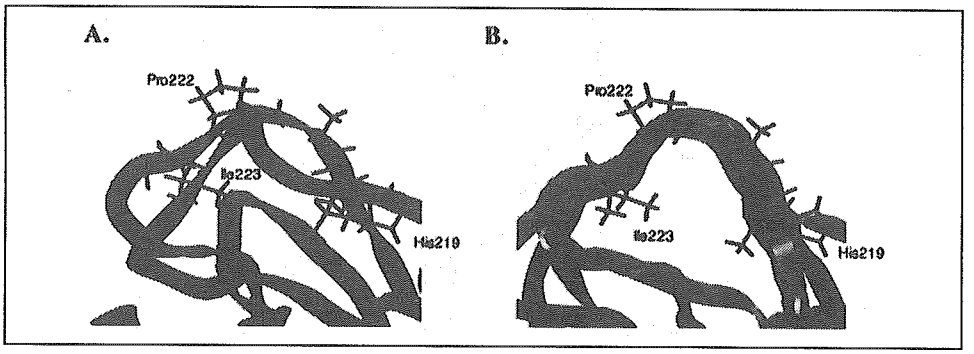

FIGURE 7. **Loop conformations of CA_{WT} and CA_{MT}.** *A*, ribbon diagram of CA_{P222A} (*purple*) superimposed on that of CA_{WT} (*red*). CA_{P222A} causes a significant distortion of the loop structure. The value of weighted root mean square deviation of the structure of CA_{P222A} from CA_{WT} structure is 3.16 Å. *B*, ribbon diagrams of the structures of the CypA binding region of various CA_{MT}, generated with 1-ns dynamics calculations, are superimposed on the structure of CA_{WT}. CA_{WT} is shown in *red*, CA_{H219Q} in *yellow*, CA_{H219P} in *blue*, $CA_{H219Q/P222A}$ in *magenta*, and $CA_{P222A/A224E}$ in *cyan*. *Residues 218–223 of* CA_{WT} are shown as *red sticks*. The values of weighted root mean square deviation of CA_{H219Q}, CA_{H219P}, $CA_{H219Q/P222A}$, and $CA_{P222A/A224E}$ structures from CA_{WT} structure are 0.99, 1.77, 1.24, and 1.48 Å, respectively. H219Q and H219P substitutions do not significantly affect the conformation of the CypA binding region of CA_{WT}. Note that the conformations of the CypA binding region of CA_{WT} and mutant CA species structurally resemble each other. Also note that $CA_{H219Q/P222A}$ and $CA_{P222A/A224E}$ have the conformation of the CypA binding loop region restored close to that of CA_{WT} in comparison with CA_{P222A}.

values of weighted root mean square deviation of CA_{H219Q}, CA_{H219P}, and $CA_{H219Q/P222A}$ structures from CA_{WT} structure were 0.99, 1.77, and 1.24 Å, respectively. Thus, it was thought that the restoration of the distorted conformation of the CypA binding loop caused by H219Q and P222A substitutions were presumably responsible for the improved replication compared with HIV-1_{P222A}, particularly in PHA-PBM where CypA contents are significantly less in comparison with MT-2 and H9 cells (Fig. 3 and Fig. 5, *A–D*).

As noted above, when HIV-1_{1NL4-3} was propagated in the absence of PI in MT-2 cells, the virus also acquired A224V mutation by passage 10 (4). It should be noted that Ala^{224} is also located within the CypA binding loop of p24 Gag protein and is also known to interact with CypA through hydrophobic contacts (9). Therefore, we also examined the highly intriguing findings by Braaten and co-workers (24) that the addition of A224E substitution rescued the replication of an otherwise poorly replicating HIV-1_{P222A} without increasing the level of viral CypA incorporation that had been reduced by P222A substitution. As shown in Fig. 7*B*, the loop conformation, with the two amino acid substitutions, is restored closely to that of the wild-type conformation. The values of weighted root mean square deviation of $CA_{P222A/A224E}$ structure from CA_{WT} structure was 1.48 Å. This observation should corroborate our observation that the conformation of the CypA binding region of capsid is critical for viral fitness.

DISCUSSION

It should be noted that certain polymorphic amino acid residues seen in HIV-1 strains are associated with HIV-1 drug resistance (2, 3). It is also known that certain drug resistance-conferring amino acid substitutions found in one subtype HIV-1 isolated from patients under therapy may be detected in HIV-1 of other subtypes from individuals having received no therapy (25, 26). Moreover, a recent study by Colson *et al.* (27) has revealed that HIV-2 strains harbor specific patterns of natural polymorphism and resistance. It is particularly of note that out of 88 different HIV-1 strains compiled in the HIV Sequence Compendium 2000 (22), 65 had histidine at position 219, whereas13 had glutamine, and 4 had proline. Hence, as studied in this work both Gln^{219} and Pro^{219} represent polymorphic amino acid residues, and it is thought that these

two polymorphic amino acids are associated with the acquisition of resistance to certain PIs.

In the present study, we found that the two substitutions H219Q and H219P were closely associated with replication advantages when propagated in CypA-rich MT-2 and H9 cells. The same advantage was seen in PHA-PBM containing a smaller amount of CypA, but only in a limited fashion (Fig. 2 and Fig. 3, *A* and *B*). We also found that these substitutions reduced CypA incorporation into virions (Fig. 3*C*), which is compatible with previous reports by two groups (28, 29). It was therefore postulated that MT-2 and H9 cells contained high CypA amounts, thereby compromising HIV-1_{WT} replication. However, H219Q and H219P substitutions apparently reduced the viral interaction with CypA, resulting in enhanced HIV-1 replication (Figs. 2 and 3). Most interestingly, when HIV-1_{H219Q} was exposed to CsA (0.5 μM), its replication was suppressed, unlike that of HIV-1_{WT}, and the higher CsA concentration (2.5 μM) further suppressed HIV-1_{H219Q} replication in all the cell preparations examined (Fig. 4). It is noteworthy that Braaten *et al.* (5) reported that virion-associated CypA amounts were reduced by 50 and 75% when HIV-1 was propagated in the presence of 0.5 and 2.5 μM CsA, respectively. Although the exact role of CypA in HIV-1 replication is as yet unclear, CypA seems to play a critical role early in the HIV-1 replication cycle (5, 8, 30) by destabilizing the capsid (p24)-capsid interactions, thereby promoting disassembly of the viral core (9). An excessive depletion of CypA may tighten capsid-capsid binding, thereby interfering with virion uncoating and reducing HIV-1 replication rates, although such a sequel is speculative at present. On the other hand, higher amounts of CypA may greatly destabilize capsid-capsid interactions, thereby rendering the virion core unstable and likewise decrease HIV-1 replication (23). Thus, it was thought that the CsA-induced HIV-1_{H219Q} replication reduction in MT-2 and H9 cells was because of an excessive depletion of CypA. It is also of note that our observation that CsA potentiated HIV-1_{WT} replication in MT-2 and H9 cells, although it failed to boost HIV-1_{H219Q} replication, makes our view more plausible that H219Q substitution is directly responsible for the increased viral replication and the reduction of CypA content in daughter virions.

The presence of Pro at position 222 in p24 Gag protein has been shown to be a primary determinant of CypA binding (9), and its substitution to Ala (P222A) decreases viral CypA incorporation, causing reduced HIV-1 replication in Jurkat cells (5, 6). In this regard, HIV-1_{P222A} was originally reported to have a severely compromised infectivity in Jurkat cells (5, 6), but it was later reported that CypA-rich H9 and CEM cells could support the replication of HIV-1_{P222A} (23, 31). In the present study, we also found that the P222A substitution reduced CypA incorporation by HIV-1 by ~75% (Fig. 5*E*) and significantly reduced HIV-1 replication in Jurkat cells and PHA-PBM, which contained relatively low CypA amounts (Fig. 3, *A* and *B*). We presumed that the introduction of H219Q substitution, which decreases p24 Gag protein binding to CypA (Fig. 3*C*), to HIV-1_{P222A} would further decrease viral CypA incorporation and thereby replication. It was intriguing that the H219Q substitution added to HIV-1_{P222A} potentiated HIV-1 replication as examined in all the cell preparations used (Fig. 5, *A–D*). These data suggest either that the added H219Q substitution enabled HIV-1_{P222A} to incorporate more CypA into daughter virions or altered a conformation of the CypA binding domain of p24 Gag protein, thereby rendering the virus relatively independent of CypA. In fact, the virus-associated CypA amount in HIV-$1_{H219Q/P222A}$ was less than or comparable with that in HIV-1_{P222A} (Fig. 5*E*). It is worth noting that a substitution at position 224 of p24 Gag protein from Ala to Glu (A224E) recovers the compromised replication of HIV-1_{P222A} in Jurkat cells but does not alter the viral CypA incorporation (24). It is also worth noting that even though all the amino acid substitutions examined here decreased viral CypA incorporation, only P222A substitution decreased viral replication. We showed that the loop conformation of the CypA binding region of CA_{WT}, CA_{H219Q}, and CA_{H219P} was quite similar to each other, whereas the conformation of CA_{P222A} sustained the most distortion (Fig. 7, *A* and *B*). It should be noted that $CA_{H219Q/P222A}$ and $CA_{P222A/A224E}$ (24) not only improve viral replication over CA_{P222A} but also restored their conformation (Fig. 5, *A–D*, and Fig. 7, *A* and *B*). We postulate that the conformation of the CypA binding region of CA_{151} is strongly correlated with viral fitness, and the functional role of CypA is to maintain the conformation of CA_{151} for viral replication.

It should be noted that HIV-1 infection of simian cells is restricted at an early post-entry step by the presence of simian TRIM5α (tripartite motif 5α) (32). In this respect, replacement of HIV-1 capsid protein with simian immunodeficiency virus capsid sequence significantly reduced the simian TRIM5α-mediated restrictions, demonstrating that the capsid protein of HIV-1 is a critical viral determinant for susceptibility to post-entry restriction in simian cells (33). Most interestingly, H219Q substitution of HIV-1 capsid is reported to be associated with the reduction of simian TRIM5α-mediated restriction (34, 35), suggesting that conformational change of CypA binding loop by H219Q, as we described in this work, might reduce the recognition by simian TRIM5α. It is also possible that the effects of H219Q observed in this study involve alterations of the interaction of TRIM5α and/or TRIM5α cofactors with the HIV-1 capsid. It is noteworthy that human TRIM5α, which has been shown to partly restrict HIV-1 infection (32), may be contributing to the effects on HIV-1 replication that occur when CypA is not able to bind the capsid protein of HIV-1 (36).

In summary, our study suggests that the H219Q substitution increases HIV-1 replication through (i) maintaining the loop conformation of CypA binding region and (ii) providing favorable conditions for viral replication by reducing viral CypA incorporation. The present data also show that the replication of HIV-1 with $CA_{H219Q/P222A}$ and that with $CA_{P222A/A224E}$, as studied elsewhere (24), were restored as compared with the otherwise compromised replication of HIV-1 with CA_{P222A} by restoring the loop conformation without increasing CypA content. We believe that an optimal concentration of CypA, which is neither excessively high nor excessively low, is critical for viral fitness and that the functional role of CypA is to maintain the conformation of CA_{151}.

Acknowledgments—We are grateful to Douglas Braaten and Jeremy Luban for kindly providing the plasmid of HIV-1_{P222A}; Mark K. Kavlick for technical assistance and helpful discussion; and the Center for Information Technology, National Institutes of Health, for computational resources.

REFERENCES

1. Mitsuya, H., and Erickson, J. (1999) in *Textbook of AIDS Medicine* (Merigan, T. C., Bartlet, J. G., and Bolognesi, D., eds) pp. 751–780, Williams & Wilkins, Baltimore
2. Kavlick, M. F., and Mitsuya, H. (2001) in *Art of Antiretroviral Therapy* (De Clarcq, R., ed) pp. 279–312, American Society for Microbiology, Washington, D. C.
3. Tanaka, M., Srinivas, R. V., Ueno, T., Kavlick, M. F., Hui, F. K., Fridland, A., Driscoll, J. S., and Mitsuya, H. (1997) *Antimicrob. Agents Chemother.* **41,** 1313–1318
4. Gatanaga, H., Suzuki, Y., Tsang, H., Yoshimura, K., Kavlick, M. F., Nagashima, K., Gorelick, R. J., Mardy, S., Tang, C., Summers, M. F., and Mitsuya, H. (2002) *J. Biol. Chem.* **277,** 5952–5961
5. Braaten, D., Franke, E. K., and Luban, J. (1996) *J. Virol.* **70,** 3551–3560
6. Franke, E. K., Yuan, H. E., and Luban, J. (1994) *Nature* **372,** 359–362
7. Braaten, D., and Luban, J. (2001) *EMBO J.* **20,** 1300–1309
8. Steinkasserer, A., Harrison, R., Billich, A., Hammerschmid, F., Werner, G., Wolff, B., Peichl, P., Palfi, G., Schnitzel, W., Mlynar, E., and Rosenwirth, B. (1995) *J. Virol.* **69,** 814–824
9. Gamble, T. R., Vajdos, F. F., Yoo, S., Worthylake, D. K., Houseweart, M., Sundquist,

W. I., and Hill, C. P. (1996) *Cell* **87,** 1285–1294
10. Gross, I., Hohenberg, H., Huckhagel, C., and Krausslich, H. G. (1998) *J. Virol.* **72,** 4798–4810
11. Turner, B. G., and Summers, M. F. (1999) *J. Mol. Biol.* **285,** 1–32
12. Mimoto, T., Imai, J., Kisanuki, S., Enomoto, H., Hattori, N., Akaji, K., and Kiso, Y. (1992) *Chem. Pharm. Bull.* **40,** 2251–2253
13. Kageyama, S., Mimoto, T., Murakawa, Y., Nomizu, M., Ford, H., Shirasaka, T., Gulnik, S., Erickson, J., Takada, K., Hayashi, H., Broder, S., Kiso, Y., and Mitsuya, H. (1993) *Antimicrob. Agents Chemother.* **37,** 810–817
14. Yoshimura, K., Kato, R., Yusa, K., Kavlick, M. F., Maroun, V., Nguyen, A., Mimoto, T., Ueno, T., Shintani, M., Falloon, J., Masur, H., Hayashi, H., Erickson, J., and Mitsuya, H. (1999) *Proc. Natl. Acad. Sci. U. S. A.* **96,** 8675–8680
15. Ghosh, A. K., Kincaid, J. F., Cho, W., Walters, D. E., Krishnan, K., Hussain, K. A., Koo, Y., Cho, H., Rudall, C., Holland, L., and Buthod, J. (1998) *Bioorg. Med. Chem. Lett.* **8,** 687–690
16. Yoshimura, K., Kato, R., Kavlick, M. F., Nguyen, A., Maroun, V., Maeda, K., Hussain, K. A., Ghosh, A. K., Gulnik, S. V., Erickson, J. W., and Mitsuya, H. (2002) *J. Virol.* **76,** 1349–1358
17. Kimpton, J., and Emerman, M. (1992) *J. Virol.* **66,** 2232–2239
18. Kosalaraksa, P., Kavlick, M. F., Maroun, V., Le, R., and Mitsuya, H. (1999) *J. Virol.* **73,** 5356–5363
19. Tamiya, S., Mardy, S., Kavlick, M. F., Yoshimura, K., and Mitsuya, H. (2004) *J. Virol.* **78,** 12030–12040
20. Kaminski, G. A., Friesner, R. A., Tirado-Rives, J., and Jorgensen, W. J. (2001) *J. Phys. Chem.* **105,** 6474–6487
21. Still, W. C., Tempczyk, A., Hawley, R. C., and Hendrickson, T. (1990) *J. Am. Chem. Soc.* **112,** 6127–6129
22. Kuiken, C., Foley, B., Hahn, B., Marx, P., McCutchan, F., Mellors, J. W., Mullins, J., Wolinsky, S., and Korber, B. (2000) in *Human Retroviruses and AIDS* (Bradac, J., ed) pp. 201–298, Los Alamos National Laboratory, Los Alamos, NM
23. Yin, L., Braaten, D., and Luban, J. (1998) *J. Virol.* **72,** 6430–6436
24. Braaten, D., Aberham, C., Franke, E. K., Yin, L., Phares, W., and Luban, J. (1996) *J. Virol.* **70,** 5170–5176
25. Cornelissen, M., van den Burg, R., Zorgdrager, F., Lukashov, V., and Goudsmit, J. (1997) *J. Virol.* **71,** 6348–6358
26. Quinones-Mateu, M. E., Albright, J. L., Mas, A., Soriano, V., and Arts, E. J. (1998) *J. Virol.* **72,** 9002–9015
27. Colson, P., Henry, M., Tourres, C., Lozachmeur, D., Gallais, H., Gastaut, J. A., Moreay, J., and Tamalet, C. (2004) *J. Clin. Microbiol.* **42,** 570–577
28. Li, Q., Moutiez, M., Charbonnier, J. B., Vaudry, K., Menez, A., Quemeneur, E., and Dugave, C. (2000) *J. Med. Chem.* **43,** 1770–1779
29. Yoo, S., Myszka, D. G., Yeh, C., McMurray, M., Hill, C. P., and Sundquist, W. I. (1997) *J. Mol. Biol.* **269,** 780–795
30. Thali, M., Bukovsky, A., Kondo, E., Rosenwirth, B., Walsh, C. T., and Sodroski, J. (1994) *Nature* **372,** 363–365
31. Ackerson, B., Rey, O., Canon, J., and Krogstad, P. (1998) *J. Virol.* **72,** 303–308
32. Stremlau, M., Owens, C. M., Perron, M. J., Kiessling, M., Autissier, P., and Sodroski, J. (2004) *Nature* **427,** 848–853
33. Owens, C. M., Yang, P. C., Göttlinger, H., and Sodroski, J. (2003) *J. Virol.* **77,** 726–731
34. Owens, C. M., Song, B., Perron, M. J., Yang, P. C., Stremlau, M., and Sodroski, J. (2004) *J. Virol.* **78,** 5423–5437
35. Kootstra, N. A., Münk, C., Tonnu, N., Landau, N. R., and Verma, I. M. (2003) *Proc. Natl. Acad. Sci. U. S. A.* **100,** 1298–1303
36. Towers, G. J., Hatziioannou, T., Cowan, S., Goff, S. P., Luban, J., and Bieniasz, P. D. (2003) *Nat. Med.* **9,** 1138–1143

JBC Papers in Press. Published on February 13, 2006 as Manuscript M512688200
The latest version is at http://www.jbc.org/cgi/doi/10.1074/jbc.M512688200

STRUCTURAL AND MOLECULAR INTERACTIONS OF CCR5 INHIBITORS WITH CCR5

Kenji Maeda[1,2,3], Debananda Das[3], Hiromi Ogata-Aoki[1,2], Hirotomo Nakata[1,2], Toshikazu Miyakawa[2], Yasushi Tojo[1,2], Rachael Norman[3], Yoshikazu Takaoka[4], Jianping Ding[5], Eddy Arnold[5], and Hiroaki Mitsuya[1,2,3]

From [1]Department of Hematology and [2]Department of Infectious Diseases, Kumamoto University Graduate School of Medical and Pharmaceutical Sciences, Kumamoto 860-8556, Japan; [3]Experimental Retrovirology Section, HIV and AIDS Malignancy Branch, National Cancer Institute, Bethesda, MD 20892, USA; [4]Minase Research Institute, Ono Pharmaceutical Co. Ltd., Osaka 618-8585; [5]Center for Advanced Biotechnology and Medicine, and Chemistry and Chemical Biology Department, Rutgers University, Piscataway, NJ 08854, USA.

Running Title: Interactions of CCR5 inhibitors with CCR5

Address correspondence to: Hiroaki Mitsuya, Department of Infectious Diseases, Kumamoto University Graduate School of Medical and Pharmaceutical Science, 1-1-1 Honjo, Kumamoto 860-8556, Japan, Tel. (+81) 96-373-5156; Fax. (+81) 96-363-5265; E-Mail: hmitsuya@helix.nih.gov

We have characterized the structural and molecular interactions of CC-chemokine receptor 5 (CCR5) with three CCR5 inhibitors active against R5 human immunodeficiency virus type 1 (HIV-1) including a potent *in vitro* and *in vivo* CCR5 inhibitor aplaviroc (AVC). The data obtained with saturation binding assays and structural analyses delineated the key interactions responsible for the binding of CCR5 inhibitors with CCR5 and illustrated that their binding site is located in a predominantly lipophilic pocket in the interface of extracellular loops (ECLs) and within the upper transmembrane (TM) domain of CCR5. Mutations in the CCR5 binding sites of AVC decreased gp120 binding to CCR5 and the susceptibility to HIV-1 infection, while mutations in TM4 and TM5 that also decreased gp120 binding and HIV-1 infectivity had less effects on the binding of CC-chemokines, suggesting that CCR5 inhibition targeting appropriate regions might render the inhibition highly HIV-1-specific while preserving the CC chemokine-CCR5 interactions. The present data delineating residue-by-residue interactions of CCR5 with CCR5 inhibitors should not only help design more potent and more HIV-1-specific CCR5 inhibitors, but also give new insights into the dynamics of CC-chemokine-CCR5 interactions and the mechanisms of CCR5 involvement in the process of cellular entry of HIV-1.

Highly active antiretroviral therapy (HAART) has brought about a major impact on the acquired immunodeficiency syndrome (AIDS) epidemics in industrially advanced nations (1,2), however, eradication of HIV-1 appears to be currently impossible mainly due to the viral reservoirs remaining in blood and infected tissues (3). Successful antiviral drugs, in theory, exert their virus-specific effects by interacting with viral components such as viral genes or their transcripts without disturbing cellular metabolisms or functions (2). However, at present, no antiretroviral drugs or agents have been demonstrated to be completely specific for HIV-1 and devoid of toxicity or side effects in the therapy of AIDS (4). Limitations of antiviral therapy of AIDS are exacerbated by complicated regimens, emergence of drug resistant HIV-1 variants (1), and a number of inherent adverse effects (5).

Thus, identification of new antiretroviral drugs which have unique mechanisms of action and produce no or least minimal side effects remains an important therapeutic objective

(2,4). CCR5 is a member of G protein-coupled, seven- transmembrane segment receptors (GPCRs), which comprise the largest superfamily of proteins in the body (6). In 1996, it was revealed that CCR5 serves as one of the two essential co-receptors for HIV-1 entry to human $CD4^+$ cells, thereby serving as an attractive target for possible intervention of HIV-1 infection (7-10). Aplaviroc (AVC; AK602/ONO4128/873140; Fig. 1), a novel spirodiketopiperazine derivative, represents a CCR5 inhibitor which specifically binds to human CCR5 with a high affinity, greatly blocks HIV-1-gp120/CCR5 binding, and exerts potent activity against a wide spectrum of laboratory and primary R5-HIV-1 isolates including multi-drug resistant $HIV\text{-}1_{MDR}$ (IC_{50} values of 0.2-0.6 nM) (11). AVC, despite its much greater anti-HIV-1 activity than other previously published CCR5 inhibitors including TAK-779 and SCH-C (Fig. 1), preserves RANTES and MIP-1β binding to $CCR5^+$ cells and their functions, while TAK-779 and SCH-C fully block the CC-chemokines/CCR5 interactions (11). AVC reportedly has an extensive and prolonged CCR5 occupancy as examined in phytohemagglutinin-activated peripheral blood mononuclear cells ($T_{1/2}$ ~9 hr) (12) and in circulating lymphocytes in HIV-1-negative and HIV-1-positive individuals ($T_{1/2}$ of 69-152 hr depending on different AVC doses)(S. Sparks *et al.*, 12th Conference on Retroviruses and Opportunistic Infections, abstr. 77, 2005). In a randomized, placebo-controlled short-term monotherapy trial in patients with AIDS including those who were drug-experienced, AVC demonstrated potent antiretroviral activity and brought about significant reduction in HIV-1 viremia (by ~ 1.7 log) in AIDS patients (J. Lalezari *et al.*, 44th Interscience Conference on Antimicrobial Agents and Chemotherapy, abstr. H-1137b, 2004).

In the present study, we examined the profile of binding to and interactions with CCR5 of three CCR5 inhibitors, AVC, SCH-C and TAK-779. We also conducted structural analyses of the interactions of CCR5 inhibitors with CCR5, using homology modeling, robust structure refinement, and docking. Notably, the molecular modeling analyses were combined and fine-tuned with the results of the saturation binding assay using a panel of mutant CCR5-expressing cells and ^{3}H-CCR5 inhibitors and the resultant configurations and orientations of inhibitors docked within the hydrophobic cavity of CCR5 yielded structure-activity predictions and interpretations consistent with the observed experimental data. The present approach of combining the site-directed mutagenesis-based data and molecular modeling should represent a valuable strategy for gaining structural insights for membrane-bound proteins for which X-ray crystal structures are not as yet available. The present data delineating residue-by-residue interactions of CCR5 with CCR5 inhibitors should not only help design more potent and more HIV-1-specific CCR5 inhibitors, but also give new insights into the dynamics of CC-chemokine-CCR5 interactions and the mechanisms of CCR5 involvement in the process of cellular entry of HIV-1.

Experimental Procedures

Reagents - A CCR5 inhibitor, aplaviroc (AVC), was designed and synthesized as previously published (11). Two other CCR5 inhibitors, TAK-779 and SCH-351125 (SCH-C) were synthesized based on the previously published structures (13,14)(Fig. 1). These three CCR5 inhibitors were tritiated by reductive amination with sodium triacetoxyborotritide (15), methylation with [^{3}H]methyliodide, and/or heterogeneous catalytic exchange with tritium gas (16). Two ^{125}I-labeled chemokines [macrophage inflammatory protein-1α (MIP-1α) and regulated upon activation, normal T cell expressed and secreted (RANTES)] were purchased from Amersham Pharmacia Biotech (Little Chalfont, UK) and ^{125}I-labeled macrophage inflammatory protein-1β (MIP-1β) was purchased from PerkinElmer Life Sciences, Inc. (Boston, MA). Their corresponding unlabeled chemokines were purchased from PeproTech Inc. (Rocky Hill, NJ). Recombinant $HIV\text{-}1_{YU2}$ gp120 (rgp120) and human soluble CD4 (sCD4) were purchased from Immuno Diagnostics, Inc. (Woburn, MA).

Cells and Viruses - The Chinese hamster ovary (CHO) cells overexpressing CCR5 (17) were maintained in Ham's F-12 medium (GIBCO-BRL, Rockville, MD) supplemented with 10% fetal calf serum (FCS: JRH Biosciences, Lenaza, KS) and 50 U/ml penicillin and 50 μg/ml streptomycin in the presence of 5 μg/ml blasticidin S hydrochloride.

The HeLa-CD4-LTR-β-gal indicator cell line expressing human CCR5 [$CCR5^+$MAGI (multinuclear activation of galactosidase indicator) cells] (18) was a kind gift from Dr. Yosuke Maeda, Kumamoto University Graduate School of Medical and Pharmaceutical Sciences, Japan. $CCR5^+$MAGI cells were maintained in Dulbecco's modified Eagle's medium (DMEM) supplemented with 10% FCS, 200 μg/ml G418, 100 μg/ml hygromycin B, and 100 μg/ml zeomycin. The U373-MAGI cell line was obtained from the AIDS Research and Reference Reagent Program, NIAID, National Institutes of Health (Bethesda, MD). U373-MAGI cells were maintained in DMEM supplemented with 10% FCS, 200 μg/ml G418, and 100 μg/ml hygromycin B. An R5-HIV-1 strain, HIV-1_{BaL}, was employed for the determination of the susceptibility of mutant CCR5 ($CCR5_{MT}$)-expressing cells to the infectivity of HIV-1.

Generation of wild type and $CCR5_{MT}$-overexpressing cells - A mammalian expression vector pZeoSV2 (Invitrogen, Carlsbad, CA) carrying human wild type CCR5 ($CCR5_{WT}$) gene (pZeoSV-CCR5) (18) was a kind gift from Dr. Yosuke Maeda. A variety of plasmids carrying a mutant CCR5-encoding gene were generated using the site-directed mutagenesis technique employing QuickChange site-directed mutagenesis kit (Stratagene, La Jolla, CA) as described by the manufacturer. Mutations introduced into the CCR5 gene were introduced through: (i) substitution of an amino acid(s) or (ii) deletion of an amino acid(s) at selected amino acid positions of CCR5. A mutation from Gly to Arg at position 163, where the corresponding amino acid in simian CCR5 is Arg, was also introduced. This G163R substitution has been reported to reduce the binding of R5-HIV-1-gp120 to human CCR5 and the susceptibility to HIV-1 (19). All these plasmids were confirmed to contain only desired mutation(s) by nucleotide sequencing.

CHO cells (or U373-MAGI cells) were transfected with a plasmid containing $CCR5_{WT}$-encoding gene or a plasmid carrying a $CCR5_{MT}$-encoding gene using Lipofectamine (Gibco BRL); the transfectants were magnetically sorted, following treatment with an anti-CCR5 monoclonal antibody (2D7 or 3A9; BD PharMingen, San Diego, CA), using Dynabeads M-450 coupled to goat anti-mouse IgG (Dynal A.S. Oslo, Norway); and the cells were cloned using the limiting dilution technique.

Determination of CCR5 expression levels in CHO and U373-MAGI cells - CCR5 expression levels of various clones described above were determined using three indicators: (i) maximal amounts of ^{3}H-AVC bound to cells (B_{max}); (ii) mean florescence intensity (MFI) values when stained with monoclonal antibody (mAb) 3A9; and (iii) MFI values when stained with mAb 2D7. The antigenic epitope for 2D7 is located distant from that for 3A9 (20) and 3A9 does not compete with AVC binding to CCR5 (data not shown). The expression levels were expressed as % control ($CCR5_{WT}$-expressing cells as control), and the highest value obtained was chosen as the estimated CCR5 expression level. There were no clones which had low values in all three indicators, thus sustaining that the current method used for CCR5 expression levels was thought to be legitimate. CD4 and CCR5 expression levels were also determined using the quantitative fluorescence-activated cell sorting (QFACS) assay system (Quantum Simply Cellular Kit; Sigma, Saint Louis, MO) using 3A9 and 2D7 (12). For the HIV-1 susceptibility assay, U373-MAGI clones which expressed CD4 molecules ranging 10-25 x 10^4 antigen-binding sites (ABS) were selected. $CCR5_{MT}$-expressing CHO cells were maintained in Ham's F-12 medium containing 10% FCS and 100 μg/ml zeomycin. $CCR5_{WT}$- and $CCR5_{MT}$-expressing U373-MAGI cells were cultured in a DMEM supplemented with 10% FCS, 200 μg/ml G418, 100 μg/ml hygromycin B, and 100 μg/ml zeomycin.

Saturation binding assay using ^{3}H-labeled CCR5 inhibitors - Saturation binding assay using ^{3}H-labeled CCR5 inhibitors was conducted and the K_D (dissociation constant) values of CCR5 inhibitors in $CCR5_{WT}$-, or $CCR5_{MT}$-expressing CHO cells were calculated as previously described (11).

Radiolabeled inhibitor binding/competition studies – $CCR5_{WT}$-expressing cells (1.5 x 10^5) were plated onto 48-well microculture plates, incubated for 24

hrs, rinsed, exposed to ^{3}H-AVC, ^{3}H-SCH-C, or ^{3}H-TAK-779 for 15 min at room temperature, subsequently exposed to various concentrations of unlabelled CCR5 inhibitors, incubated for 30 min, thoroughly washed, lysed, and the radioactivity in the lysates was counted. All experiments were performed in duplicate. The amounts of each ^{3}H-labeled CCR5 inhibitor bound to the cells are shown as mean % control values. Standard deviation (SD) values are indicated with the vertical lines. To obtain control values, the experiment was also performed without the addition of unlabelled CCR5 inhibitors.

Determination of CC-chemokine- and HIV-1 gp120-binding affinity to $CCR5_{WT}$ and $CCR5_{MT}$ - Binding profiles of chemokines to $CCR5_{WT}$- or $CCR5_{MT}$-expressing cells were determined using ^{125}I-labeled chemokines as previously reported (11) with minor modifications. In brief, $CCR5_{WT}$- or $CCR5_{MT}$-expressing cells (1.5×10^{5}) were plated onto 48-well microculture plates, incubated for 24 hrs, rinsed, exposed to 5 nM ^{125}I-MIP-1α, ^{125}I-MIP-1β, or ^{125}I-RANTES at room temperature for 1 hr, thoroughly washed with PBS, lysed with 0.5 ml of 1N NaOH, and the radioactivity in the lysates was counted. The non-specific binding of the labeled chemokine to the cells was determined based on the radioactivity detected in the wells plated with the same number of CCR5-negative CHO (CHO-K1) cells exposed to an equal amount of ^{125}I-labeled chemokine. Determination of the binding profiles of HIV-1-rgp120 to $CCR5_{WT}$ or $CCR5_{MT}$ was also conducted. Briefly, $CCR5^{+}$CHO cells were exposed to rgp120 (5 μg/ml) and sCD4 [5 μg/ml: biotinylated using EZ-link sulfo-NHS-SS-biotin (Pierce, Rockford, IL)] for 1 hr at 37°C. Cells were washed and the binding of the rgp120-sCD4 complex to $CCR5^{+}$CHO cells was determined using phycoerythrin-conjugated streptavidin (SA-PE: BD PharMingen). Non-specific binding was determined based on the MFI of SA-PE with sCD4 but without rgp120. Since CCR5 expression levels vary among CCR5 clones, the % binding (occupancy) values for ^{125}I-chemokines and rgp120 were normalized using the following formula: % binding (occupancy) = 100 x [amount of ^{125}I-chemokine or rgp120 bound to $CCR5_{MT}$/amount of ^{125}I-chemokine or rgp120 bound to $CCR5_{WT}$]x[number of $CCR5_{WT}$ /number of $CCR5_{MT}$], where numbers of $CCR5_{WT}$ and $CCR5_{MT}$ are expressed as B_{max} (cpm) or MFI values as described above.

Determination of HIV-1 susceptibility of $CCR5_{WT}$- and $CCR5_{MT}$-expressing cells - The susceptibility of $CCR5_{WT}$- and $CCR5_{MT}$-expressing cells to the infection by an R5-HIV-1 strain, $HIV\text{-}1_{BaL}$, was determined as previously described (22). In brief, target cells ($CCR5_{WT}$- or $CCR5_{MT}$-expressing U373-MAGI cells; 10^{4}/well) were plated onto 96-well flat microtiter culture plates, inoculated with 100 $TCID_{50}$ of $HIV\text{-}1_{BaL}$ on the following day, cultured for 48-72 hrs, stained with 400 μg/ml of X-gal, and all blue cells were counted. All experiments were performed in triplicate. For testing each of $CCR5_{MT}$-expressing cell preparations, multiple (5 to 13) clones were examined. In each set of experiments, $CCR5_{WT}$-clone #1 was included and served as a standard. Percent infection in $CCR5_{WT}$- and $CCR5_{MT}$-expressing cells was determined using the following formula: % Infection = 100 x (mean blue cell number in a well)/(mean blue cell number in a well of $CCR5_{WT}$-clone #1).

Structural modeling of the interactions of CCR5 inhibitors with wild-type and mutant CCR5 species - An initial structural model of CCR5 was defined with homology modeling using the crystal structure of bovine rhodopsin as a template (23). This resulted in the initial placement of the helices and side chains. The CCR5-inhibitor complex structures were defined with an iterative optimization of CCR5 and inhibitor structures in the presence of each other, using software tools from Schrödinger (Schrödinger, LLC, New York, NY 2005), as described below. The conformational flexibility of both CCR5 and the inhibitors were taken into account. The molecular structures of AVC, SCH-C, and TAK-779 were obtained by minimization using the MMFF94 force field (24). For each minimized inhibitor configuration, a set of low energy structures was generated by performing a Monte Carlo sampling of their conformations. Thus obtained structures were used as starting structures for docking calculations where their conformations were further refined.

The protonation states of CCR5 residues were assigned, and residues more than 20 Å from the active site were neutralized. In an attempt to place an inhibitor within CCR5, initially the active site was artificially enlarged by mutating Tyr108, Cys178, Glu283, and Met287 to Ala. The van der Waals radii of inhibitor atoms were scaled by a factor of 0.70 to reduce steric clashes and docked into CCR5. After obtaining an initial set of CCR5-inhibitor complexes, residues 108, 178, 283, and 287 were mutated back from Ala to their original states. CCR5 atoms within 15 Å of an initially placed inhibitor were subsequently refined. It was achieved by using the rotamer library of Xiang and Honig (25) and optimizing each side chain one at a time holding all other side chains fixed. After convergence, all side chains were simultaneously energy minimized using the OPLS-AA force field (26) to remove any remaining clashes. The inhibitors were docked again and scored to estimate their relative affinity. The docked complexes with higher scores were visually examined along with the mutational data to select the best possible CCR5-inhibitor complex.

Mutated CCR5 structures were defined using wild type CCR5 structure and optimized using the OPLS2003 force field. Charges were taken from the force field. The minimization was carried out until the gradient was below 0.2 kJ/Å-mol. Resulting minimized structures were used as starting structures for obtaining docked complexes of mutated CCR5 with inhibitors using the protocol described above. Visualization, structural refinement, and docking were performed using Maestro 7.0, MacroModel 9.0, Prime 1.2, Glide 3.5, and IFD script from Schrödinger, LLC (New York, NY 2005). The extra-precision mode of Glide, which has higher penalty for unfavorable and unphysical interactions, was used (27). Computations were carried out on a multiprocessor SGI Origin 3400 computer platform.

A probe radius of 1.4 Å with Connolly surfaces generated was used to define binding site cavities using the method of Exner *et al.* (28) as implemented in the MOLCAD tool in Sybyl 7.0 (Tripos, Inc., St. Louis, MO). Lipophilic potential was mapped onto the cavities using parameters from Viswanadhan *et al.* (29).

RESULTS

Site-directed mutagenesis of CCR5 and binding affinity of CCR5 inhibitors – We have previously reported (11) that AVC competitively blocked the binding of a monoclonal antibody, 45531, which is known to be specific against the C-terminal half (or domain B) of the second extracellular loop (ECL2B) of CCR5 (21) while AVC failed to block or only partially blocked the binding of two other monoclonal antibodies, 2D7 and 45523, specific for CCR5 but not for its ECL2B. When we examined three additional monoclonal antibodies, 3A9 and 45502 (both specific for NH_2-terminus) and 45549 (multi-domain-reactive)(20,21), none of these antibodies were replaced by AVC (data not shown). These data suggest that the potent inhibitory activity of AVC against R5 HIV-1 infection stems from its binding to ECL2B and/or its vicinity with high affinity.

In an attempt to delineate the CCR5 binding profile of the three CCR5 inhibitors, we generated a variety of CCR5 mutant-overexpressing ($CCR5_{MT}$) CHO cells and determined the K_D values of each inhibitor to mutant CCR5 species using the saturation binding assay with tritiated inhibitors. When we determined the K_D value of AVC with respect to a CCR5 mutant carrying an Asp to Ala substitution at position 11 of the amino-terminus domain ($CCR5_{D11A}$), the value was 3.0 nM, virtually identical to the K_D value with wild-type CCR5 ($CCR5_{WT}$; Table I), indicating that the D11A substitution did not affect the binding of AVC to CCR5. The K_D value of AVC with respect to $CCR5_{Y37A}$ was moderately greater with 7.9 nM (2.7-fold compared to the K_D value with regard to $CCR5_{WT}$). On the other hand, those of TAK-779 and SCH-C to $CCR5_{Y37A}$ were 98.9 nM (3.3-fold compared to the K_D with regard to $CCR5_{WT}$) and >200 nM (>12.5-fold), respectively, in agreement with the previous reports in which both TAK-779 and SCH-C apparently failed to bind, probably explaining that these inhibitors failed to block HIV-1 infection of $CCR5_{Y37A}$-expressing cells (30,31). These data suggest that the binding of TAK-779 and SCH-C to $CCR5_{WT}$ is more dependent on interactions with Tyr37 than that of AVC. We also generated a series of CCR5-overexpressing CHO cells carrying a mutation(s) at a selected amino acid position(s).

As shown in Table 1, the mutations which substantially (more than 3-fold compared to AVC binding to $CCR5_{WT}$) affected the K_D values of AVC were as follows: Y108A and F113A in the third transmembrane domain (TM3) of CCR5; R168A and S180E in ECL2; K191R and K191N of the interface of ECL2B and TM5; K197A and I198A of TM5; Y251A of TM6; and M287E of TM7. The mutations which greatly diminished the binding of AVC (values of >200 nM) to CCR5 were as follows: G163R, C178A, WKNF190del, K191A, and E283A. It is worthwhile to interject that Lys191 in ECL2 is reported to be critical for the binding of RANTES, MIP-1α, and MIP-1β to CCR5 (32,33), while Cys178 is presumed to form a disulfide bond with Cys101 of ECL1 and to be critical for the conformation of CCR5 (34). Mutations which substantially affected the binding of TAK-779 and SCH-C to CCR5 were as follows: Y37A, Y108A, and E283A for TAK-779 and Y37A, WKNF190del, I198A, and E283A for SCH-C. It is noteworthy that the number of mutations that affected the binding of AVC was notably greater than those of TAK-779 and SCH-C. Thus, the CCR5 binding modes of AVC, TAK-779, and SCH-C apparently share some similar features but also have some distinct differences.

Structural analysis locates aplaviroc in the interface of ECL and TM domains – In the present study, a three-dimensional model of human CCR5-CCR5 inhibitor complex was defined by combining the results of site-directed mutagenesis-based analyses (Table 1) and molecular modeling that involved structure refinement and simultaneous docking of inhibitors to an initial structure of CCR5 based on the crystal structure of bovine rhodopsin (23). Fig. 2 illustrates the three-dimensional model of CCR5 that has a seven trans-membrane helical structure. Six hydrophobic cavities were identified in the extracellular, transmembrane, and intracellular domains of CCR5. Among them, a hydrophobic cavity to which CCR5 inhibitors highly likely to bind was identified based on its size and location (red arrow head in Fig. 2). This cavity is the largest one among the six that can accommodate a molecule of the size of AVC and other CCR5 inhibitors and is in the region implicated to have the greatest effect on K_D values with amino acid substitutions introduced in CCR5 among the six hydrophobic cavities identified. It should be noted, however, that the conformations of CCR5 without an inhibitor and CCR5 with the inhibitor can be substantially different from each other, since significant conformational changes would be expected to follow ligand binding to CCR5. Nevertheless, it is intriguing to note that this largest cavity corresponds to the binding site for the retinal ligand in bovine rhodopsin; given the propensity of this pocket to bind fairly large ligands such as the CCR5 inhibitors, it is possible that this binding cavity could accommodate some as-yet uncharacterized ligands produced in the body during the normal function of CCR5, potentially even some with regulatory roles.

Based on the set of the K_D values of AVC in relation to various mutant CCR5 species overexpressed on CHO cells (Table 1), structural analysis of AVC-CCR5 interactions was conducted, which suggested that a series of intramolecular and intermolecular hydrogen bonds occur, which should stabilize the CCR5-AVC complex. We identified a significant network of hydrogen bonds among four amino acid residues: Gly163, Ser180, Lys191, and Thr195 (Fig. 3*A*). Gly163 is located in TM4, Ser180 in ECL2, and Lys191 and Thr195 in TM5. Another network of hydrogen bonds was identified among another four amino acid residues: Tyr37, Glu283, Met287, and Tyr108 (Fig. 3*B*). Tyr37 is located in TM1, Tyr108 in TM3, and Glu283 and Met287 in TM7. These hydrogen bond networks spanning multiple domains appear to maintain the optimal shape of the cavity for the binding of AVC. Indeed, further analysis of the cavity also revealed that the ECL regions have some hydrophilic character (Fig. 4*A*, red arrow head), whereas the rest of the cavity is mostly lipophilic (Fig. 4*A*). The carboxyl and hydroxymethyl of AVC interact with the hydrophilic regions of CCR5. The rest of AVC interacts with the lipophilic region of CCR5 (Fig. 4*A-B*). It is of note that AVC has a molecular weight of 614.2, larger than TAK-779 (Mr. 531.1) and SCH-C (Mr. 557.5), has a substantial hydrophobic contact and fits well inside the large binding cavity within CCR5 as shown in Fig. 4*A*. AVC also forms hydrogen bonds with Cys178, Ser180, Lys191 and Thr195 (Fig. 3*A-B*). It is presumed that these interactions with residues in